Reducing functionally defective HSCs alleviates aging-related phenotypes in old mice

Yuting Wang[1,2,3], Wenhao Zhang[1,2,3], Chao Zhang[1,2,3],
Hoang Tran Van[1,2,3], Takashi Seino[1,2,3] and Yi Zhang[1,2,3,4,5*]

[1]Howard Hughes Medical Institute, Boston Children's Hospital, Boston, Massachusetts 02115, USA;
[2]Program in Cellular and Molecular Medicine, Boston Children's Hospital, Boston, Massachusetts 02115, USA;
[3]Division of Hematology/Oncology, Department of Pediatrics, Boston Children's Hospital, Boston, Massachusetts 02115, USA;
[4]Department of Genetics, Harvard Medical School, Boston, Massachusetts 02115, USA;
[5]Harvard Stem Cell Institute, WAB-149G, 200 Longwood Avenue, Boston, Massachusetts 02115, USA.

[*]To whom correspondence should be addressed
E-mail: yzhang@genetics.med.harvard.edu

Keywords: Aging, HSC, heterogeneity, CD150, rejuvenation

Manuscript information: 41 pages, 6 figures, 10 extended data figures, 7 supplementary tables

Abstract

Aging is a process accompanied by functional decline in tissues and organs with great social and medical consequences. Developing effective anti-aging strategies is of great significance. In this study, we demonstrated that transplantation of young hematopoietic stem cells (HSCs) into old mice can mitigate aging phenotypes, underscoring the crucial role of HSCs in the aging process. Through comprehensive molecular and functional analyses, we identified a subset of HSCs in aged mice that exhibit "youthful" molecular profiles and functions, marked by low expression levels of CD150. Mechanistically, $CD150^{low}$ HSCs from old mice can effectively differentiate into downstream lineage cells but not their $CD150^{high}$ counterparts. Notably, transplantation of old $CD150^{low}$ HSCs attenuates aging phenotypes and prolongs the lifespan of elderly mice compared to those transplanted with unselected or $CD150^{high}$ HSCs. Importantly, reducing the dysfunctional $CD150^{high}$ HSCs can alleviate aging phenotypes in old recipient mice. Thus, our study demonstrates the presence of "youthful" HSCs in old mice, and that rejuvenation can be achieved by removal of the dysfunctional HSCs.

Introduction

The aging process is marked by a functional decline across various tissues and organs[1-3], which significantly increases the risk for a multitude of chronic diseases[4]. Previous studies have shown that transfusion of young blood or its components into aged mice can have a rejuvenation effect[5-10], supporting an important role of the hematopoietic system in whole body aging. Hematopoietic stem cells (HSCs), the source of all hematopoietic cell types, undergo profound functional changes with age, including increased prevalence of clonal hematopoiesis, a shift toward myeloid-biased differentiation, and a diminished capacity for blood regeneration[11-15]. Recent studies have shown that replacing HSCs of old mice with those of young mice can improve health and extend the lifespan of the old recipient mice[16-18]. Conversely, transplanting aged HSCs into young mice can accelerate immune system aging and reduce their lifespan[19,20]. These studies highlight the hematopoietic system, and particularly HSCs, as key players in the aging process, suggesting that HSCs could serve as promising targets for aging-related intervention.

Previous research has established that intrinsic alterations of HSCs with aging are associated with their functional decline, such as increased DNA damage, mitochondrial degeneration, diminished asymmetric distribution of CDC42, altered H4K16 acetylation during mitosis, and epigenetic modifications[21-27]. Interestingly, the HSC population exhibits intrinsic heterogeneity in both young and old mice, distinguishable by lymphoid-biased, balanced, and myeloid-biased subtypes based on surface markers and lineage predispositions[28-36]. Notably, a fraction of HSCs can preserve long-term dormancy and functionality during aging[37-39]. However, the changes of HSC heterogeneity during aging and their contribution to systemic aging remains to be comprehensively characterized.

In this study, we demonstrate that transplantation of young HSCs can rejuvenate old mice. scRNA-seq reveals an increased aging heterogeneity in old HSCs. Systematic molecular and functional characterization indicated the presence of “youthful” and functionally defective “old” subsets of HSCs in old mice, marked by differential expression levels of CD150. Mechanistically, old $CD150^{high}$ HSCs exhibit differentiation defects when compared to those of the $CD150^{low}$ HSCs. Notably, transplantation of the “youthful” subset of HSCs into old recipient mice can attenuate aging phenotypes, including decreased epigenetic age and extended lifespan

of old recipient mice when compared with those that received old un-selected HSCs or CD150^{high} HSCs. Importantly, reducing the dysfunctional CD150^{high} HSCs can attenuate aging phenotypes in old recipient mice, highlighting that the removal of defective CD150^{high} HSCs from old mice could be a potential strategy for rejuvenation.

Results

Transplantation of young HSCs rejuvenates old recipient mice

To directly evaluate the functional differences between young and old HSCs *in vivo*, we sorted long-term (LT)-HSCs [lineage$^-$c-Kit$^+$Sca-1$^+$ (LSK) CD48$^-$CD34$^-$CD150$^+$] (referred to as HSCs) from young and old mice (**Extended Data Fig. 1a**). Consistent with previous reports[12,13,40], a significant increase in the number of HSCs in old mice was observed when compared with their young counterparts (**Extended Data Fig. 1b**). Serial transplantation of both young and old HSCs into lethally irradiated young recipient mice (**Fig. 1a**) followed by examination of the donor HSC chimerism in the peripheral blood (PB) revealed a notable decline in the repopulation capacity and biased differentiation of old HSCs compared to their young counterparts (**Fig. 1b and Extended Data Fig. 1c-f**). These results are consistent with previous studies[12,20], and confirm the age-related intrinsic functional decline of HSCs.

To analyze the contribution of HSCs to systemic aging, we independently transplanted young or old HSCs into irradiated middle-aged mice (13 months). After a stable engraftment of the transplanted HSCs in the peripheral blood (5 months post-transplantation), we evaluated the aging status of the recipient mice by performing blood analyses and physical tests (**Fig. 1c**). Previous studies have shown that the blood cell composition changes with aging, characterized by an increase in myeloid cells and a corresponding decrease in lymphoid cells[41,42]. Notably, mice transplanted with young HSCs exhibited a more youthful blood cell composition, characterized by increased B cell and reduced T cell and myeloid cell proportions, as well as an increase in overall white blood cells and lymphoid counts, compared to the recipients that received old HSCs (**Fig. 1d, e**). This suggests a crucial role of HSCs in systematic hematopoietic aging.

The ratio of naïve T cells serves as a critical indicator of immune function, which declines during the aging process[43]. Conversely, central memory T cells (Tcm) and effector memory T cells (Tem) exhibit an increase with aging[44], which were confirmed by our study (**Extended Data Fig. 2**). Notably, the old mice that received young HSCs have more naïve T cells in both CD4 and

CD8 T cells, indicating a rejuvenated immune system after young HSCs transplantation (**Fig. 1f and Extended Data Fig. 3a**).

The DNA methylation clock is widely used as an indicator of aging[45]. Importantly, old mice that received young HSCs transplantation have a significantly younger epigenetic age compared to those that received old HSCs (**Fig. 1g**). Consistently, old mice that received young HSCs exhibited improved physical functions when compared to those that received aged HSCs, including muscle strength (grip strength), motor coordination (pole test, beam balance and rotarod), locomotor activity (open field test) and cognitive functions (fear conditioning test), without significant difference in body weight of the recipients (**Fig. 1h and Extended Data Fig. 3b-d**). Collectively, these results demonstrate that transplantation of young HSCs to old mice can lead to whole body rejuvenation.

Single cell RNA-seq reveals a "youthful" HSC subpopulation in old mice

The above results suggest that HSCs from old mice are functionally defective compared to those from young mice. To understand the defects, we performed both bulk RNA-seq and scRNA-seq on young and old HSCs (**Fig. 2a**), which revealed a clear transcriptomic difference between young and old HSCs (**Fig. 2b and Extended Data Fig. 4a**). Bulk RNA-seq revealed 332 up-regulated genes in old HSCs, including previously annotated HSC aging marker genes [46] such as *Clu*, *Selp*, *Mt1*, *Ramp2* and *Gpr183* (**Extended Data Fig. 4a; Supplementary Table 1**). These genes were defined as HSC aging marker genes for downstream analysis. Interestingly, unsupervised clustering analysis of scRNA-seq revealed that while the quiescent young HSCs are largely uniform (only form a single cluster q4), the quiescent old HSCs can be further divided into 3 clusters (q1-3) (**Fig. 2c, d**). This result indicates that quiescent old HSCs are transcriptionally more heterogeneous compared to young HSCs.

We then identified marker genes for each of the clusters (**Fig. 2e; Supplementary Table 2**). Intriguingly, although q1-q3 are all from old HSCs, the known aging marker genes, such as *Mt1*, *Prtn3*, *Nupr1*, *Plscr2*, *Cavin2*, *Sult1a1*, *Clu*, *Ramp2*, *Alcam*, *Selp* and *Gpr183*, are highly expressed in q1 and q2 clusters, but not in q3 cluster (**Fig. 2e**). In contrast, both q3 clusters and q4 (young HSCs) clusters share highly expressed genes, despite the q3 clusters originating from old mice. GO analysis of q3 marker genes revealed an enrichment of cell proliferation related

pathways (**Fig. 2e**), which were also enriched in the young HSCs compared to old HSCs based on bulk RNA-seq (**Extended Data Fig. 4b**, aging-down). We further calculated the relative expression levels of q1, q2, and q3 marker genes in old and young HSCs, and found that the q1 and q2 marker genes are expressed significantly higher in old HSCs, while q3 marker genes are higher in young HSCs (**Fig. 2f**), supporting that q3 HSCs have a younger transcriptome than those of q1 and q2 HSCs.

To gain further support for the notion that a subset of HSCs from old mice are "youthful" in their transcriptome, we analyzed the UMAP distribution of some well-known HSC aging marker genes (*Sbspon*, *Gpr183*, *Clu*, *Ramp2*) [46] and found that they are expressed at a higher level in q1 and q2 compared to that in q3 (**Fig. 2g**). In contrast, the young HSC marker genes, such as *Rnase6* and *Arhgap30*, exhibited an opposite expression pattern (**Extended Data Fig. 4c**). To quantify the aging heterogeneity of old HSCs, we calculated the aging score, a measure of the aging-related transcriptome, for each single cell using the 332 aging marker genes identified in our bulk RNA-seq (**Supplementary Table 1**) or the top 100 HSCs aging genes previously identified (**Supplementary Table 3**)[46]. Both analyses indicate that cluster q3 has a lower aging score than q1 and q2, despite all cells originating from the same old mice. (**Fig. 2h and Extended Data Fig. 4d**). Collectively, comparative scRNA-seq revealed increased aging heterogeneity in old HSCs and a subset of old HSCs have a youthful transcriptome.

CD150 can serve as an aging heterogeneity marker for old HSCs

To better understand the aging heterogeneity of old HSCs and to assess its contribution to overall body aging, a unique cell surface marker that facilitates the separation of "youthful" from "old" cells in aged HSCs is needed. To this end, we first identified the top 150 genes showing strong correlation with aging scores in scRNA-seq (**Extended Data Fig. 5a**) and compared them with the 332 genes upregulated in old HSCs (**Extended Data Fig. 4a**), resulting in 54 shared genes (**Fig. 3a; Supplementary Table 4**). We further required membrane location for sorting purposes, which reduced the candidate gene list to 26 (**Fig. 3a**). Furthermore, the potential marker genes should have lower expression levels in q3 than in q1 and q2, which further narrowed the list to 7 (**Extended Data Fig. 5b**). Considering the availability and specificity of the antibodies, CD150 (*Slamf1*) was selected as the marker for aging heterogeneity of old HSCs.

FACS analysis of HSCs from young and old mice indicated that the population of HSCs with higher CD150 levels significantly increases with aging (**Fig. 3b**), supporting the use of CD150 levels as an indicator of aging heterogeneity in old HSCs.

To further confirm that the CD150 level can serve as a marker of aging heterogeneity of old HSCs, we separated old HSCs into 4 groups (G1 to G4) by FACS based on CD150 levels and profiled their transcriptomes (**Fig. 3c**). We then calculated the expression correlation between CD150 and each gene and identified 131 and 103 genes that exhibit strong positive or negative correlation with CD150 level in aged HSCs, respectively (**Extended Data Fig. 5c; Supplementary Table 5**). Notably, the genes that positively correlate with CD150 include many known HSC aging markers, such as *Sbspon, Ehd3, Clu, Dpy19l2, Kcnb2, Selp, B3gnt8, Jam2* and *Enpp5*. In contrast, the negatively correlated genes include genes that are highly expressed in young HSCs, such as *Serpinb1a, Usp6nl, Lrr1, Col4a2, Gng2* and *Kif15* (**Extended Data Fig. 5d**). These results suggest that CD150 level can be a potential indicator of HSC transcriptome age.

Using the 131 genes that positively correlate to the CD150 level (referred to as CD150 feature genes), we calculated the CD150 feature score for each cell and found that q3 HSCs have a significantly lower CD150 feature score than q1 and q2 HSCs (**Extended Data Fig. 5e, f**). Notably, a strong correlation between the CD150 feature score and aging score was observed (**Fig. 3d**). This indicates that the aging heterogeneity of old HSCs can be well reflected by CD150 feature genes. Consistently, HSC aging-related up- and down-regulated genes in the 4 groups of HSCs from G1 to G4 exhibit a trend that is similar to the aging process (**Fig. 3e**), confirming the positive correlation between CD150 level and HSC aging status in old mice. Furthermore, previous studies indicated that CD150 level can mark HSC subsets with different differentiation bias in both young and old mice[30,32], supporting our selection of CD150 to mark the aging heterogeneity of old HSCs.

CD150^{low} HSCs have younger epigenome with superior functions in old mice

Epigenetic changes are believed to be one of the drivers of the aging process[47-49]. To further determine whether the CD150 level can reflect epigenetic aging status in old HSCs, we first

compared the epigenetic age of old CD150^{high} and CD150^{low} HSCs by analyzing their DNA methylation profiles. Notably, CD150^{low} HSCs have a significantly lower epigenetic age than that of CD150^{high} HSCs despite that they are derived from the same old mice (**Fig. 3f**). Given that stem cell aging is accompanied by chromatin accessibility changes,[50-52] we compared the chromatin accessibility landscapes of old CD150^{low} and CD150^{high} HSCs, as well as young and old HSCs by performing ATAC-seq analyses. We found that 4,694 peaks displayed increased chromatin accessibility and 3,842 peaks showed decreased accessibility in aged HSCs relative to young HSCs. Interestingly, a similar change between CD150^{low} and CD150^{high} old HSCs was also observed around the aging-related open and closed ATAC-seq peaks (**Fig. 3g**). These results indicate that CD150 can serve as a marker reflecting both transcriptional and epigenetic aging in aged HSCs.

Previous studies have shown that increased DNA damage and decreased percentage of cells in proliferation are associated with functional decline of old HSCs [27,53,54]. Interestingly, we observed an increase of double stranded breaks (indicated by γH2AX) as well as a decrease in the proportion of cells in proliferation for CD150^{high} compared to CD150^{low} old HSCs (**Extended Data Fig. 5g, h**). This indicates that CD150^{low} HSCs may have better function than CD150^{high} HSCs in old mice.

To directly compare the function between old CD150^{low} and CD150^{high} HSCs, we performed serial competitive transplantation (**Fig. 3h**). We found that CD150^{low} old HSCs have significantly better engraftment capacity compared to their CD150^{high} counterparts in both the first and second transplantation (**Fig. 3i and Extended Data Fig. 6**). These results demonstrate that CD150 not only marks transcriptome and epigenome heterogeneity but also functional heterogeneity of old HSCs with CD150^{low} HSCs having better function than CD150^{high} HSCs.

Although young HSCs exhibit a homogeneous transcriptome (**Fig. 2d**) and aging score (**Fig. 2h**), their CD150 levels are variable (**Fig. 3b**). This raised the question whether CD150^{low} HSCs are also functionally superior to CD150^{high} HSCs in young mice. To address this question, we checked the cell cycle and performed similar HSC transplantation experiments using HSCs from young mice (**Extended Data Fig. 7a, b**). Consistent with their transcriptome and aging score

homogeneity, no significant functional difference was observed between CD150^{low} and CD150^{high} young HSCs for cell cycle analysis or PB chimerism during the period of 120 days after transplantation (**Extended Data Fig. 7a, c**). However, we noted a significantly higher contribution of CD150^{high} HSCs to myeloid cells, along with an upward trend in PB chimerism when compared to CD150^{low} young HSCs. These results indicate that CD150^{high} HSCs from young mice have comparable or even better function than CD150^{low} HSCs, which is in contrast with those in old mice.

Old CD150^{high} HSCs are defective in differentiation, but not in self-renewal or activation

We next attempted to dissect the mechanism underlying the differential repopulation capacity of CD150^{low} and CD150^{high} HSCs in old mice. Considering that the capabilities of self-renewal and differentiation are the two major features of stem cells, we compared both features after their transplantation. We first determined the differentiation dynamics by analyzing the differentiation state of old HSCs at different time points after transplantation (**Extended Data Fig. 8a**). We found that transplanted old HSCs start to differentiate on day 7, and the progenitor subpopulation becomes apparent on day 10 (**Extended Data Fig. 8b**). Based on this information, we separately transplanted old CD150^{low} and CD150^{high} HSCs and analyzed the donor derived hematopoietic stem and progenitor cells (HSPCs) in bone marrow on days 7 and 14 after transplantation (**Fig. 4a**). Notably, we found that CD150^{high} HSCs showed a significantly lower ratio in short term HSCs (ST-HSCs) and multipotent progenitors (MPPs), but a higher ratio in LT-HSCs compared to CD150^{low} HSCs (**Fig. 4b and Extended Data Fig. 8c**), indicating that old CD150^{high} HSCs might have differentiation and/or activation (quiescent to activated state) defects compared to CD150^{low} HSCs.

To determine whether old CD150^{high} HSCs exhibit an activation defect, we profiled transcriptomes of CD150^{low} and CD150^{high} HSCs 4 days after transplantation when the HSCs had yet to initiate differentiation but were under stimulation (**Extended Data Fig. 8d**). By comparing with freshly isolated HSCs (without activation), we identified 794 commonly up-regulated genes in both CD150^{low} and CD150^{high} HSCs after transplantation (**Extended Data Fig. 8e; Supplementary Table 6**). The commonly up-regulated genes are highly enriched in terms related to cellular division. Consistently, the G2M checkpoint related genes were similarly

upregulated in both CD150^{low} and CD150^{high} HSCs upon transplantation (**Extended Data Fig. 8f**). These results indicate that old CD150^{high} HSCs can be effectively activated as CD150^{low} HSCs following transplantation.

We further compared the proliferation capacity of old CD150^{low} and CD150^{high} HSCs in culture (**Extended Data Fig. 8g**) and found that old CD150^{low} and CD150^{high} HSCs exhibited comparable proliferation rates (**Extended Data Fig. 8h, i**). Taken together, these results indicate that impaired repopulation capacity of old CD150^{high} HSCs are caused by defective differentiation, but not activation or proliferation.

To rule out a possible delay in differentiation of old CD150^{high} HSCs after transplantation, we analyzed the persistence of the differentiation and self-renewal capacity of old CD150^{high} HSCs over an extended period of 5 months. We co-transplanted old CD150^{low} or CD150^{high} HSCs (GFP negative) with competitors (GFP positive) and analyzed the differentiation and chimerism of donor HSCs in both bone marrow and PB 5 months later (**Fig. 4c**). We observed a consistent differentiation defect of old CD150^{high} HSCs when compared to their CD150^{low} counterparts when analyzing donor derived HSPCs in the bone marrow (**Fig. 4d**). Additionally, the donor chimerism of old CD150^{high} HSCs exhibits a clear trend of decline from LT-HSCs through ST-HSCs, MPPs, to PB, while the donor chimerism of old CD150^{low} HSCs remains relatively stable (**Fig. 4e**), supporting a long-term differentiation defect of old CD150^{high} HSCs.

Collectively, these results indicate a long-lasting impairment in differentiation, but not in activation or self-renewal of old CD150^{high} HSCs, which explains the diminished repopulation capacity of this subpopulation.

Old CD150^{high} HSCs are defective in the LT-HSCs to ST-HSCs transition

To determine the specific stage when the differentiation defects of old CD150^{high} HSCs occur, we performed comparative scRNA-seq analysis of the HSPCs derived from old CD150^{low} and CD150^{high} HSCs 14 days after transplantation. We obtained 2,406 and 1,925 high quality HSPCs derived from transplanted CD150^{low} and CD150^{high} HSCs, respectively (**Fig. 4f**). Cell cycle phase analysis indicated that similar proportions of HSPCs derived from CD150^{low} and

CD150^{high} HSCs were actively cycling (**Extended Data Fig. 8j**), consistent with our conclusion that CD150^{low} and CD150^{high} HSCs can be similarly activated by transplantation (**Extended Data Fig. 8e, f**).

Based on the expression of the HSPC marker genes [50,55] and the HSPC sorting markers (*Ly6a*, *Kit*, *Cd34*, *Cd48* and *Slamf1*), the 4,331 HSPCs can be divided into 7 subclusters that include LT-HSC-like, ST-HSC-like, MPP2-like, MPP3-like, MPP4-like, GMP-like and MEP-like cells (**Fig. 4g and Extended Data Fig. 8k**). When HSPCs derived from CD150^{low} and CD150^{high} HSCs were compared, we found that HSPCs derived from CD150^{high} HSCs were significantly enriched in LT-HSC-like cells compared to those derived from CD150^{low} HSCs (**Fig. 4g, h**), consistent with our FACS analysis (**Fig. 4b and Extended Data Fig. 8c**). Since the proportions of CD150^{low} and CD150^{high} HSCs derived ST-HSCs are comparable, our data indicate that the differentiation defects of CD150^{high} HSCs were mainly at the stages of LT-HSC to ST-HSC, and ST-HSC to MPP4 transitions. Given that MPP4 are the major progenitor cells of the lymphoid lineage, the substantial decrease in the MPP4 population might be a major cause of the biased differentiation of CD150^{high} HSCs[30,32]. Collectively, comparative bone marrow scRNA-seq analysis of transplanted old HSCs indicated that the differentiation defects of old CD150^{high} HSCs is caused by a block of LT-HSCs to ST-HSCs transition.

The "youthful" subset of old HSCs can alleviate aging phenotypes and extend lifespan

Transplantation of young HSCs as an anti-aging therapy is impractical for humans due to immune incompatibility among different individuals. The demonstration that HSCs in old mice have molecularly and functionally "youthful" CD150^{low} HSCs prompted us to ask whether this subset of HSCs can help to attenuate aging phenotypes of old mice. To this end, we transplanted CD150^{low}, whole HSCs (un-selected), or CD150^{high} HSCs from old mice into 13-month-old recipients and analyzed aging phenotypes 5 months later (**Fig. 5a**). Compared to recipients that received whole-HSCs and CD150^{high} HSCs, mice transplanted with CD150^{low} HSCs showed higher percentage of B cells, and lower percentage of T cells and myeloid cells (**Fig. 5b**), as well as increased blood cell numbers, including lymphoid cells, neutrophils, eosinophils and red blood cells (**Fig. 5c**). Importantly, a significant increase in the naïve T cell ratio and a decrease in Tcm and Tem ratios in the CD8^{+} (**Fig. 5d**) and CD4^{+} (**Extended Data Fig. 9a**) T cells were also

observed in mice that received CD150^{low} HSCs relative to those that received whole-HSCs or CD150^{high} HSCs. These results suggest that transplantation of old CD150^{low} HSCs can improve both hematopoiesis and immune parameters in old mice.

To determine whether improved hematopoiesis and immune parameters can benefit physical performance, we performed a series of tests that measure muscle strength (grip strength, wire hanging), coordination (beam balance, pole test), and endurance (rotarod and treadmill). Consistently, we found a general trend of degrading physical performance in the order of CD150^{low}, whole-HSCs, and CD150^{high} HSCs (**Fig. 5e**) without significant differences in their body weight (**Extended Data Fig. 9b**). In almost all cases, mice transplanted with old CD150^{low} HSCs performed significantly better than those transplanted with CD150^{high} HSCs. Consistent with improved physical performance, we found that old mice that received CD150^{low} HSCs display a lower epigenetic age (**Fig. 5f**). Importantly, aged recipient mice transplanted with old CD150^{low} HSCs exhibited a substantial lifespan extension, achieving a 9.2% and 11.7% increase in median lifespan compared to counterparts transplanted with whole-HSCs or CD150^{high} HSCs (**Fig. 5g**).

Taken together, our results indicate that not only transplantation of young HSCs, but the molecularly and functionally "youthful" subset of old HSCs can attenuate aging phenotypes of old mice. Considering that the functionally defective CD150^{high} HSCs increase with aging, our results raise the possibility that rejuvenation might be achieved by reducing or removing the functionally defective HSCs from old mice.

Reducing the dysfunctional HSCs can alleviate aging phenotypes in old recipient mice

To assess whether reducing defective HSCs in old mice can enhance hematopoiesis and mitigate aging-related phenotypes, we conducted the following transplantation experiment: 500 old CD150^{low} HSCs were co-transplanted to irradiated middle-aged (13 months) mice with 2,500 (1:5 ratio), 1,000 (1:2 ratio) and 0 (1:0 ratio) CD150^{high} old HSCs in order to mimic whole-HSC, partial removal, and complete removal of CD150^{high} HSCs, respectively. Five months after the transplantation, we assessed the hematopoietic system and physical capabilities of recipient mice to compare the aging status of the three groups (**Fig. 6a**). The 1:5 ratio serves as a control, which

is determined based on the percentage of q3 to the total HSC in old mice revealed by scRNA-seq (**Fig. 2d**).

Peripheral blood analysis indicated that compared to the 1:5 group, the 1:2 and 1:0 groups have increased percentage of B cells and decreased percentage of myeloid cells (**Fig. 6b**). Complete blood counting analysis also showed higher number of whole white blood cells, neutrophils, and lymphoid cells in the 1:0 and 1:2 groups compared to the 1:5 group (**Fig. 6c**). Importantly, increased naïve $CD4^+$ and $CD8^+$ T cells, as well as decreased effective memory T cells were also detected in the 1:2 and 1:0 groups compared to the 1:5 group (**Fig. 6d and Extended Data Fig. 10a**), indicating the presence of the defective $CD150^{high}$ HSCs has adverse effects on the "youthful" functional $CD150^{low}$ HSCs for hematopoiesis and immune function in old mice.

Next, we examined whether reducing the $CD150^{high}$ HSCs ratio can improve physical functions of the recipient mice by performing a multitude of physical tests. The results indicate consistent improved physical functions in the 1:2 and 1:0 groups compared to the 1:5 group, including muscle strength (grip strength), motor coordination (pole test, beam balance, and rotarod), and locomotor activity (open field test), with no notable differences in body weight (**Fig. 6e and Extended Data Fig. 10b**). These findings not only confirm the adverse effect of the defective $CD150^{high}$ HSCs in aged mice, but also suggest that their reduction in old mice can ameliorate aging-related phenotypes.

It is important to note that the 1:2 group exhibited a significantly younger and healthier hematopoietic system, immune parameters, and enhanced physical functions compared to those of the 1:5 group. This observation indicates that anti-aging effects can be accomplished by partial elimination of defective HSCs in aged mice, highlighting its application potential since partial removal is much more practical than complete removal.

Discussion

By transplantation, we demonstrated a key role of HSCs in systematic aging (**Fig. 1**). Integrating scRNA-seq and functional evaluation, we identified a "youthful" subset of HSCs in old mice that is marked by low level of CD150 (**Fig. 2 and 3**). Comparative analysis demonstrated that CD150^{high} HSCs from old mice are defective in LT-HSC to ST-HSC differentiation when compared with the CD150^{low} HSCs (**Fig. 4**). Importantly, transplantation of the "youthful" CD150^{low} HSCs can alleviate aging phenotypes and extend the lifespan in old mice (**Fig. 5**). Finally, we provide evidence demonstrating that the hematopoietic system and physical performance of old recipient mice can be improved by reducing the ratio of functionally defective CD150^{high} HSCs (**Fig. 6**), raising the possibility that rejuvenation can be achieved by removing the dysfunctional HSCs in the elderly.

CD150 level as an indicator of aging heterogeneity in old HSCs

scRNA-seq revealed that while quiescent HSCs in young mice are relatively homogeneous, the counterpart in old mice are heterogenous (**Fig. 2d, h**). By analyzing the genes highly expressed in "older" subpopulations of aged HSCs, we identified CD150 (gene *Slamf1*) as a cell surface marker that can serve as an indicator of HSC aging in transcriptome, epigenome and functions in old HSCs (**Fig. 2 and 3**). Originally characterized as a surface marker for LT-HSCs[56], CD150 has also been used to reflect differentiation bias of HSCs in young and old mouse[30,32]. Additionally, CD150^{low} HSCs from aged mice have been shown to retain normal lymphoid differentiation capacity when removed from the aged microenvironment[34]. These previous results suggest a potential link between CD150 levels and HSC function during aging and are in line with our results, which further support CD150 as a marker of HSC aging heterogeneity.

In addition to CD150, we have identified other cell surface proteins, such as *Lpar6*, *Ehd3* and *Tm4sf1*, that can also mark the "older" populations in old HSCs (data not shown). Interestingly, during the preparation of this manuscript, Kim *et al*. reported that *Clca3a1* can also serve as a marker to capture the HSC heterogeneity in old mice. They found that Clca3a1^{high} HSCs from aged mice have a decreased repopulation capacity in primary transplantation and exhibited a myeloid-biased differentiation compared to Clca3a1^{low} HSCs[31]. However, this functional

difference between Clca3a1^{high} and Clca3a1^{low} old HSCs was not maintained in the second transplantation. In contrast, the functional difference between CD150^{high} and CD150^{low} old HSCs persisted in the second transplantation (**Fig. 3i**), indicating that CD150 is a more robust indicator of the functional heterogeneity of aged HSCs. *Clca3a1* was not in our potential marker gene list due to its minimal expression difference between q3 and q1+q2 clusters in our scRNA-seq analysis (data not shown).

The "youthful" subset of old HSCs is functional in alleviating aging phenotypes

Our results, along with previous research in mice, demonstrate that transplantation of young HSCs is promising for anti-aging treatments (**Fig. 1**)[16-19]. However, transplantation of young HSCs as an anti-aging therapy is impractical in humans due to immune rejection. By combining scRNA-seq with functional analysis, we identified a "youthful" subset of HSCs in old mice that is marked by lower level of CD150 (**Fig. 2 and 3**). Comparative analyses further demonstrated that this subset of HSCs is superior to the whole-HSCs or CD150^{high} HSCs in terms of: 1) balanced differentiation (**Fig. 5b**); 2) absolute blood cells numbers (**Fig. 5c**); 3) immune system quality (**Fig. 5d**); 4) physical functions (**Fig. 5e**); 5) epigenetic age (**Fig. 5f**) and 6) lifespan (**Fig. 5g**). These results support the notion that transplantation of a "youthful" subset from old donors has anti-aging effects. Given that these "youthful" HSCs reside in aged individual, immune rejection is not an issue. The demonstrated rejuvenation effect of this "youthful" HSC population found in old mice could serve as a potential source for anti-aging therapies should this observation also be true in humans.

Removal of dysfunctional HSCs in old as a way of rejuvenation

Since the discovery of the rejuvenating effects of young blood through parabiosis,[7] great efforts have been spent on searching for rejuvenation factors from young blood. Although modulating several candidate factors, such as CDC42, SELP, CCL5, PHF6, IGF1, PF4 and the Yamanaka factors (Oct4, Sox2, Klf4, c-Myc) have been reported to have rejuvenating effects during the past years,[23,46,57-63] their rejuvenating capacities are limited and the mechanisms underlying their rejuvenating effects are not clear. In some cases, such as GDF11, conflicting results were also reported.[9,10,64,65] Thus far, no universally accepted rejuvenating factors have been identified. Our findings reveal that old HSCs exhibit molecular and functional heterogeneity, comprising

"youthful" and dysfunctional "old" subsets (**Fig. 4 and 5**). Moreover, reducing the proportion of dysfunctional HSCs ameliorates aging phenotypes in aged mice after transplantation (**Fig. 6**), suggesting that removal of functionally defective HSCs from old could be a promising approach for rejuvenation. Consistent with this notion, a very recent study showed that depletion of the myeloid-biased HSCs (marked by NEO1) by a specific antibody cocktail could restore immune functions in old mice[66], although whether their approach can lead to a systemic body rejuvenation remains unknown. Nevertheless, our study and this recent report have set the stage for achieving rejuvenation in the elderly by targeted removal of dysfunctional HSCs.

Material and methods

Mice

All experiments were conducted in accordance with the National Institute of Health Guide for Care and Use of Laboratory Animals and approved by the Institutional Animal Care and Use Committee (IACUC) of Boston Children's Hospital and Harvard Medical School. For bulk and single-cell RNA-seq, 2-3 months young and 22-24 months old C57BL/6 mice were used (Jackson Lab #00664). For HSC transplantation, 2-3 months old young (Jackson Lab #00664) or 2-3 months old GFP+ young (Jackson Lab #006567) mice were used. For competitive transplantation, competitor HSCs were collected from 3-4 months GFP+ young (Jackson Lab #006567) mice. Except specially mentioned, the recipient mice were B6 CD45.1 mice (Jackson Lab #002014), and the helper cells were also collected from B6 CD45.1 mice. For old recipient mice, 13 months old wild type (Jackson Lab #00664) were used. The helper cells were from age-matched wild type mice.

LT-HSCs sorting and transplantation

Bone marrow (BM) cells were collected by crushing tibias, femurs, pelvic bone and spine (spinal cord was removed). The resulting cell suspension was filtered through 70 µm cell strainers and red blood cell were lysed with red blood cell lysis buffer (ebioscience catalog #00-4333-57). To improve the sorting efficiency, filtered cells were further enriched by removing lineage positive cells. For detail, the filtered cells were first stained with biotin-conjugated antibodies against lineage markers (CD4, CD8, Gr-1, CD11b, CD5, B220 and Ter119). Lineage positive cells were removed by streptavidin-conjugated magnetic beads (STEMCELL catalog #19856), and the lineage negative cells were further stained with antibodies against mouse c-Kit, Sca-1, CD48, CD34, CD150. The dead cells were labeled with DAPI. The LT-HSCs were defined as $Lin^{-}Sca\text{-}1^{+}c\text{-}Kit^{+}CD48^{-}CD34^{-}CD150^{+}$. To prepare helper cells, bone marrow cells were collected from long bones (tibias and femurs) of CD54.1 mice (Jackson Lab #2014) by flushing. After lysing red blood cells, all HSPCs were removed by Sca-1 positive selection kit (STEM CELL catalog #18756). The remaining cells were counted and used as helper cells for transplantation.

For transplantation experiments, a specific number of LT-HSCs were sorted with FACS sorter (SONY SH800). Sorted LT-HSCs were mixed with 3×10e5 helper cells and transplanted into lethally irradiated (9.5 Gy) recipient mice (Jackson Lab #2014) using 1ml syringe attached with a 27.5-gauge needle.

Cell cycle and DNA damage marker γH2AX analysis of HSCs with FACS

The analysis of cell cycle status of HSCs was performed as pervious described[67]. Briefly, bone marrow cells were prepared, enriched, and stained with HSC marker antibodies as mentioned before. Then the enriched bone marrow cells were fixed and permeabilized with BD Intra Kit (#641776). After washing, fixed HSCs were stained with monoclonal antibody against mouse KI67 (eBioscience, #11-5698-80) and Hoechst33342 (Thermo Scientific, #R37165) or with antibody against DNA damage marker γH2AX (Cell Signaling Technology, #9719S). The cell cycle state of HSCs or DNA damage marker γH2AX levels were analyzed with FACS after washing.

Bulk RNA-seq library

Bulk-RNA sequencing library is constructed based on Smart-seq2[68]. SMART-Seq v4 Ultra Low Input RNA Kit for Sequencing (Takara catalog #634890) was used and experiments were performed according to manufacturer's instructions. Briefly, sorted HSCs were incubated in lysis buffer with RNase inhibitor on dry ice for 1 minutes, and then thawed at room temperature. First-Strand Buffer, SMART-Seq v4 Oligonucleotide, 3' SMART-Seq CDS primer II and RNase inhibitor were added into the lysed cells and incubated at 72°C for 3 min before being put on ice. Incubating was performed after adding SMARTScribe II Reverse Transcriptase as following: 42°C for 90 minutes then 70°C for 10 minutes. Without purification, SeqAmp PCR Buffer, PCR Primer II A and SeqAmp DNA Polymerase were added for pre-amplification using thermal cycler for 12 cycles following the manufacturer's instruction. The amplified cDNA was then purified by 1.8× volume of SPRIselect beads (Beckman Coulter catalog #B23318). Next, 200pg cDNA was used for library preparation with Nextera XT DNA Library Preparation Kit (Illumina catalog # FC-131-1024) according to manufacturer's instruction.

scRNA-seq library preparation

Single-cell RNA seq library is prepared with Chromium Next GEM Single Cell 3' Reagent Kits V3.1 (Dual Index) from 10X Genomics according to manufacturer's instruction and previously described method.[69] Briefly, single HSCs were sorted by FACS into PBS solution. Then, microfluids was used to construct droplets containing single-cell, GEMs and reverse transcription reagents. 100 µl of droplets were incubated at 53°C for 45 minutes, then at 85°C for 5 min. Droplets were then released by Recovery Agent, cleaned up with Dynabeads MyOne SILANE and amplified by PCR for 12 cycles. The amplified cDNA was used for library construction according to the manufacturer's instruction.

Peripheral blood analysis via FACS

For PB analysis, up to 30 µL vein blood was collected from retro orbital sinus or tail tips into EDTA-coated tubes. Red blood cells were first removed by red blood cell lysis buffer (ebioscience catalog #00-4333-57). The remaining white blood cells were stained with mixed monoclonal conjugated antibodies (CD45.1, CD45.2, CD3, B220, Gr-1 and CD11b). After incubation in 4°C and darkness for 30 min, PB were analyzed by FACS (BD FICR canto-II).

HSC culture *in vitro*

Sorted LT-HSCs were cultured in StemSpan™ SFEM II (STEM CELL catalog #09605) with 10 ng/ml SCF (PeproTech, catalog #AF-250-03), 100 ng/ml TPO (PeproTech, catalog #315-14), 25 ng/ml Flt3L (PeproTech, catalog #250-31L) and 25 ng/ml IL3 (PeproTech, catalog # 213-13). Six days after culture, the number of HSCs were quantified by FACS (BD FICR canto-II).

Complete blood counting analysis of recipient mice

For whole mouse blood analysis, 75 µL vein blood was collected from retro orbital sinus and mixed with 225 µL 5mM EDTA (Research Products International, catalog #E14000-250.0). Freshly collected whole blood was analyzed by Hematology system (ADVIA 120) within 2 hours after collection.

Naïve T, Tcm and Tem analysis

We analyzed the ratio of Naïve T cells, Tcm and Tem based on a pervious report.[70] Briefly, PB was collected and red blood cells were removed by red blood cell lysis buffer (ebioscience

catalog #00-4333-57). The remaining cells were stained with antibodies against CD45.1, CD45.2, CD4, CD8, CD44 and CD62L. T cell subtypes were defined as follows: naïve ($CD62L^{high}$ $CD44^{low}$), Tcm ($CD62L^{high}$ $CD44^{high}$) and Tem ($CD62L^{low}$ $CD44^{high}$).

Reduced-representation bisulfite sequencing (RRBS) library preparation for HSCs

FACS sorted HSCs were lysed at 50°C for 3 hours and 75°C for 30 min in a 5 µl lysis buffer [20 mM tris-EDTA (Sigma catalog #T9285-100ML), 20 mM KCl (Thermo Scientific, catalog # AM9640G), 0.3% Triton X-100 (Sigma catalog # 93443-100ML), and protease (1 mg/ml; Qiagen catalog # 19155)]. The lysed cells were then subject to Msp I digestion at 37°C for 3 hours and 80°C for 20 min. Following enzymatic digestion, end-repair mix [1 µl Klenow frag exo (5 U/µl), 0.2 µl of 10×TangoBuf, and 0.8 µl of dNTP mix] was added and incubated at 37°C for 40 min and 75°C for 15 min. For adaptor ligation, the reaction was incubated at 16°C for 30 min, 4°C overnight, and 65°C for 20 min after adding the ligation mix [2.25 µl of H_2O, 1 µl of T4 ligase (30 U/µl; Thermo Scientific, catalog # EL0013), 0.5 µl of 100 mM ATP (Thermo Scientific, catalog # R0441), and 0.75 µM methylated adaptor. Bisulfite conversion reaction was then performed by the EpiTect Bisulfite Kit (Qiagen catalog #59104) following the manufacturer's instructions. Adapter-tagged BS-DNA was then amplified by 16 cycles using Kapa HiFi Uracil+ ReadyMix (Kapa Biosystems, catalog #KK2801) with NEBNext Multiplex Oligos for Illumina (New England BioLabs catalog # E7500L).

ATAC-seq library construction

About 500 ~ 1000 cells were sorted by FACS to 10 µl tagmentation buffer (33 mM Tris-Acetate, 66 mM K-Acetate, 10 mM Mg-Acetate, 16% Dimethylformamide, and 0.02% Digitonin). 0.5 µl Tn5-Adapter complex (Diagenode) was added after FACS sorting and incubated at 37°C for 30 min. Then, the tagmentation reaction was stopped by adding 10 µl stop buffer (100 mM Tris-HCl pH8.0, 100 mM NaCl, 0.4% SDS, 40 µg/ ml Proteinase K) and the samples were incubated at 55°C overnight to release the tagmentation fragments. SDS was then quenched by adding 5 µl 25% Tween-20 and incubated on ice for 10 min. Next, 25 µl samples were mixed with 30 µl NEBNext High- Fidelity 2X PCR Master Mix (NEB), 2.5 µl P5 primer (10 µM) and 2.5 µl P7 primer (10 µM) for PCR amplification. The PCR products were then purified with SPRI beads with 1:1.6 ratio (96 µl beads) before sequencing.

Physical function tests

For grip strength test, mice were gently placed on the top of a grid strength meter (Bioseb, Model GT3) so that only their forepaws could grasp the grid. The tail of the mouse was pulled three times and then returned to the cage for at least 1 min rest. We performed 2 series of pulls, averaged the top 3 animals' maximum grip strength, and normalized for body weight for each mouse.

For the beam balance test, home-made equipment was used. Briefly, a 1-meter-long smooth wood strip is elevated to 50 cm tall from the table. A black box (20×20×20 cm) is put on the plate at one end and the mouse is put at the other end. For training day, a thicker pole is used (28 mm diameter). We trained each mouse until they could go through the pole and to the box without dropping. The next day, the mice were tested with a thicker pole or a thinner pole (17 mm diameter) 3 times per mouse. Before being used for another test, the pole and box were cleaned with 70% ethanol. The latent time for the mice to go through the pole was recorded.

For pole test, mice were placed at the top of a 50 cm grooved metal pole with a diameter of 1 cm with the mice head pointing down. The time from initial placement on the top of the pole to the time the mouse reached the base of the pole (forelimb contact with platform) was recorded with a stopwatch. Following a 30-min rest in their home cage, the trial was repeated another 2 times. The average time is calculated as the latent time to go down for each mouse.

The rotarod test was used to evaluate motor coordination and balance. Mice were placed in separate lanes on the rod rotating at an initial speed of 4 rpm/min in an accelerating Rotarod system (Ugo Basile Apparatus). On the first day, each mouse finished a training program at speed of 4rpm/min for 5 min and repeated another 2 times with a 20 min interval. For the test day, the apparatus was set to accelerate from 4 to 40 rpm/min in 5 min. The time and speed were recorded when the mice dropped or consecutive two rounds of passive rotation. One or two tests per day for each mouse were performed with an interval of at least 30 min. The test was continued on the next day, and lasted for 3 tests in total. The apparatus was cleaned between mice to make sure it was dry and clean. Results were the average over 3 tests.

For the wire hanging test, the mice were placed on a metal grid with a 1-cm square mesh 50 cm above a cushioned surface covered with approximately 3-cm thick bedding. First, the mice were put on the salamander and then the salamander was inverted slowly. Start the stopwatch when the mouse was attached upside down. The latent time for the mouse to fall was recorded. With 30 min interval, each mouse was tested 3 times and results were the average over 3 trials.

For treadmill fatigue test, the protocol was adapted and modified from a previous publication.[71] Briefly, mice were acclimatized to the treadmill (Columbus Instruments Exer 3/6 Treadmill) for 2 consecutive days prior to testing. The fatigue zone was set as one mouse body-length from the shock grid. On day 1, mice were placed on the treadmill and allowed to explore for 5 min with the shock grid turned off. After 5 min, the shock grid was powered on at 1.5 mA, 3 Hz and the speed was set to 6 m/min for 5 min. After 5 min, the speed increased 2 m/min for every 2 min. The treadmill was stopped the treadmill when the mice ran at 10 m/min for 5 min. On day2, the same training program was completed except the top speed was 12 m/min for 5 min. On the test day, the speed increased stepwise over time, up to maximum of 26 m/min. The fatigue standard was met when mice are present in the fatigue zone for more than 5 seconds on three separate instances. The latency time for fatigue of each mouse was recorded for analysis.

For the fear conditioning test, we implemented contextual and cued fear conditioning (CCFC). In short, mice underwent the following training protocol on the first day: 2 minutes of acclimation, followed by a 30-second tone, then a 2-second foot shock (0.5 mA). This was followed by a 2-minute intertrial interval (ITI). Subsequently, another 30-second tone was paired with a 2-second footshock (0.5 mA), and then there was a 1-minute period before the lights went out. The following day, a context test was conducted where mice were placed in the same context for 5 minutes without any shock or tone. On the third day, mice were assessed in a modified context: 3 minutes of acclimation without tone, followed by 3 minutes with tone. Video was captured using Noduls MediaRecorder (version 4.0), and freezing behavior was analyzed using Noldus EthoVision XT17.

For the Novel Y-Maze test, the protocol is adapted from previous study[72]. Briefly, mice were pre-acclimated to a separate holding room for 30 minutes before testing. The Y-maze procedure consisted of a 3-minute habituation phase followed by a 3-minute test phase, with a strict 2-minute ITI. In the habituation phase, one arm (left or right) was obstructed, and the start arm remained consistent for each mouse. After habituation, mice were briefly returned to their holding cage during the ITI. The obstruction was then removed, and the maze was cleaned before the test phase. Then, the mouse was placed back into the start arm for the test trial and returned to the home cage after the trial was completed. Distance and time traveled in the maze were recorded and analyzed with Noldus EthoVision XT17.

For the open field test, the protocol is adapted from previous study[72]. In the open-field test, the apparatus was a transparent enclosure with a base measuring 27.3 cm by 27.3 cm and walls with a height of 20.3 cm. The central zone accounted for half of the total area. Prior to testing, mice were acclimated to the test environment for a minimum of 20 minutes. Each mouse was then positioned in the center of the arena to begin the assessment. Movements were tracked for a duration of 20 minutes and data were collected in intervals of 5 minutes using a tracking system (Med Associates, St. Albans, VT, ENV-510). Analysis included standard locomotor activity parameters such as total distance moved, average speed, active and inactive periods, as well as vertical events in the first 10min.

RNA-seq data analysis

For bulk RNA-seq datasets (**Supplementary Table 7**), adaptor of all sequenced reads was first trimmed by Trim Galore with parameter “-illumina -paried”. Then the filtered reads were aligned to the mm10 reference genome by Hisat2 (version 2.0.0-b)[73] with parameters “--no-mixed --no-discordant --dta-cufflinks --no-unal”. The aligned SAM files were then converted to BAM files with Samtools (version 1.14)[74] for further analysis. Next, HTSeq-count (V0.12.4)[75] was used to calculate the count of reads for each gene, with the main parameters set as: -f bam -s no -r pos. The reference genome was downloaded from the USCS Table Browser. To quantify gene expression, the read count for each gene was normalized using DESeq2 (V1.22.2).[76] The differentially expressed genes from each group were filtered with following criteria: adjusted P-value < 0.05 and fold-change >2 or <0.5.

ATAC-seq analysis

For ATAC-seq datasets (**Supplementary Table 7**), sequencing adaptors and low-quality reads were removed by Trim Galore with parameters: -q 20 --length 30 --paired. Then the clean reads were mapped to mouse reference genome (mm10) by bowtie2 (Version 2.5.1) with parameter: "-N 1 -L 25 -X 2000 -no-discordant" (ATAC-seq). After converting aligned SAM to BAM files using Samtools (Version 1.13), Picard (Version 2.26.4) was used for removing PCR duplications. Next, read counts were normalized by Reads Per Kilobase per Million mapped reads (RPKM) and converted to bigwig via bamCoverage (Version 3.5.1). The peaks were called by MACS2 (Version 2.2.7.1)[77] with parameter "-t file -f BED -g mm -outdir OUTPUT -n NAME --nomodel --nolambda" (ATAC-seq). The "norrowpeak" files were used for downstream analysis. The peaks that overlap in more than 60% of the replicate samples in each group were kept for feature counts and subsequent analysis using DiffBind (V3.0.15).[78] The read counts for each peak were normalized using DESeq2 (V1.30.1).[76] Peaks that differed significantly between groups were identified using DESeq2 with the following criteria: P-value < 0.05 and fold-change > 1.5 or < 0.67. Deeptools (Version 3.5.1)[79] was used to visualize the read coverages at peak regions.

scRNA-seq data analysis

Paired reads from single-cell RNA seq (**Supplementary Table 7**) were first aligned to mm10 reference genome with Cellranger --count (version 3.0.2) from 10X Genomics. Transcriptome annotation composed of protein coding genes was download and processed from Ensembl (released-102). To eliminate low-quality single cells, we filtered out single cells with feature numbers below 800 for freshly isolated HSCs (**Fig. 2**) and below 2,000 for short-term transplanted HSCs (**Fig. 4**). Additionally, cells with mitochondrial transcripts accounting for more than 5 percent were also removed. Then, the remaining single cells were processed and analyzed with Seurat (V4.0.2).[80] The young and old single cell data is first merged and then normalized and scaled. Two thousand variable feature genes were identified and used for UMAP presentation. For aging score and CD150 score calculation, the genes used are listed in Supplementary Tables 1, 3 and 5.

Epigenetic age calculation

Paired fastq files from RRBS seq (**Supplementary Table 7**) were first merged and processed as a single file. Adaptors of all sequenced reads were trimmed by Trim Galore with parameters "-illumina". Adaptor trimmed reads were mapped using Bismark (v0.20.0)[81] using parameters "--fastq -L 30 -N 1 --non_directional". Methylated CpGs were interpreted by bismark_methylation_extractor with parameter "-s --no_overlap --report -bedGraph". For base resolution 5mC level calculation, a cutoff of minimal 3× coverage was required for each CpG site. The 5mC level for certain CpG was calculated using the number of methylated CpGs to divide the number of total CpGs detected on the CpG site. Epigenetic age was calculated based on the identified sites and parameters from a previous study.[82]

Data accession

All data have been deposited to GEO with the accession number GSE233879. Access to the data by the reviewers can be achieved with the link below using token "ynadskqcxvmdbal" (GSE233879) (https://www.ncbi.nlm.nih.gov/geo/query/acc.cgi?acc=GSE233879).

Acknowledgements

We thank Jiayi Li for her assistance in some experiments. We thank the support of Mouse Behavior Core of Harvard Medical School and its director Dr. Barbara Caldarone. This project was supported by the Milky Way Research Foundation and the Howard Hughes Medical Institute (HHMI). Y.Z. is an investigator of the HHMI. This article is subject to HHMI's Open Access to Publications policy. HHMI lab heads have previously granted a nonexclusive CC BY 4.0 license to the public and a sublicensable license to HHMI in their research articles. Pursuant to those licenses, the author-accepted manuscript of this article can be made freely available under a CC BY 4.0 license immediately upon publication.

Author Contributions

Y.Z. conceived and supervised the project; Y.W., W.Z. and Y.Z. designed the experiments; Y.W. performed the cell sorting, transplantation, FACS analysis, and physical function tests with help from H.T.V.; W.Z. and Y.W. performed the library preparation for bulk RNA-seq, scRNA-seq, RRBS and ATAC-seq; Y.W., W.Z. and C.Z. analyzed the single-cell RNA-seq data; Y.W. and

W.Z. analyzed the bulk RNA-seq and RRBS data; Y.W. and C.Z. analyzed the ATAC-seq data; T.S. helped for complete blood counting analysis; Y.W., W.Z. and Y.Z. interpreted the data and wrote the manuscript with feedback from all authors.

Competing Interests

The authors declare the following competing financial interests: Yi Zhang and Yuting Wang are the inventors of a patent related to the work presented in this manuscript. The patent number is 63472759 and the title is: “Compositions and Methods for Assessing, Treating, or Reducing Aging-Related Functional Decline”, which was filed on June 13, 2023.

References

1 Brunet, A., Goodell, M. A. & Rando, T. A. Ageing and rejuvenation of tissue stem cells and their niches. *Nat Rev Mol Cell Biol* **24**, 45-62, doi:10.1038/s41580-022-00510-w (2023).

2 Rando, T. A. & Jones, D. L. Regeneration, Rejuvenation, and Replacement: Turning Back the Clock on Tissue Aging. *Cold Spring Harb Perspect Biol* **13**, doi:10.1101/cshperspect.a040907 (2021).

3 López-Otín, C., Blasco, M. A., Partridge, L., Serrano, M. & Kroemer, G. Hallmarks of aging: An expanding universe. *Cell* **186**, 243-278, doi:10.1016/j.cell.2022.11.001 (2023).

4 Kennedy, B. K. *et al.* Geroscience: linking aging to chronic disease. *Cell* **159**, 709-713, doi:10.1016/j.cell.2014.10.039 (2014).

5 Castellano, J. M., Kirby, E. D. & Wyss-Coray, T. Blood-Borne Revitalization of the Aged Brain. *JAMA Neurol* **72**, 1191-1194, doi:10.1001/jamaneurol.2015.1616 (2015).

6 Villeda, S. A. *et al.* Young blood reverses age-related impairments in cognitive function and synaptic plasticity in mice. *Nat Med* **20**, 659-663, doi:10.1038/nm.3569 (2014).

7 Conboy, I. M. *et al.* Rejuvenation of aged progenitor cells by exposure to a young systemic environment. *Nature* **433**, 760-764, doi:10.1038/nature03260 (2005).

8 Conese, M., Carbone, A., Beccia, E. & Angiolillo, A. The Fountain of Youth: A Tale of Parabiosis, Stem Cells, and Rejuvenation. *Open Med (Wars)* **12**, 376-383, doi:10.1515/med-2017-0053 (2017).

9 Katsimpardi, L. *et al.* Vascular and neurogenic rejuvenation of the aging mouse brain by young systemic factors. *Science* **344**, 630-634, doi:10.1126/science.1251141 (2014).

10 Sinha, M. *et al.* Restoring systemic GDF11 levels reverses age-related dysfunction in mouse skeletal muscle. *Science* **344**, 649-652, doi:10.1126/science.1251152 (2014).

11 Jaiswal, S. *et al.* Age-related clonal hematopoiesis associated with adverse outcomes. *N Engl J Med* **371**, 2488-2498, doi:10.1056/NEJMoa1408617 (2014).

12 Rossi, D. J. *et al.* Cell intrinsic alterations underlie hematopoietic stem cell aging. *Proc Natl Acad Sci U S A* **102**, 9194-9199, doi:10.1073/pnas.0503280102 (2005).

13 Sudo, K., Ema, H., Morita, Y. & Nakauchi, H. Age-associated characteristics of murine hematopoietic stem cells. *J Exp Med* **192**, 1273-1280, doi:10.1084/jem.192.9.1273 (2000).

14 Verovskaya, E. *et al.* Heterogeneity of young and aged murine hematopoietic stem cells revealed by quantitative clonal analysis using cellular barcoding. *Blood* **122**, 523-532, doi:10.1182/blood-2013-01-481135 (2013).

15 Jaiswal, S. & Ebert, B. L. Clonal hematopoiesis in human aging and disease. *Science* **366**, doi:10.1126/science.aan4673 (2019).

16 Das, M. M. *et al.* Young bone marrow transplantation preserves learning and memory in old mice. *Commun Biol* **2**, 73, doi:10.1038/s42003-019-0298-5 (2019).

17 Guderyon, M. J. *et al.* Mobilization-based transplantation of young-donor hematopoietic stem cells extends lifespan in mice. *Aging Cell* **19**, e13110, doi:10.1111/acel.13110 (2020).

18 Li, J. *et al.* Long-term repopulation of aged bone marrow stem cells using young Sca-1 cells promotes aged heart rejuvenation. *Aging Cell* **18**, e13026, doi:10.1111/acel.13026 (2019).

19 Guest, I., Ilic, Z., Scrable, H. & Sell, S. Survival of irradiated recipient mice after transplantation of bone marrow from young, old and "early aging" mice. *Aging (Albany NY)* **7**, 1212-1223, doi:10.18632/aging.100867 (2015).
20 Leins, H. *et al.* Aged murine hematopoietic stem cells drive aging-associated immune remodeling. *Blood* **132**, 565-576, doi:10.1182/blood-2018-02-831065 (2018).
21 Moehrle, B. M. & Geiger, H. Aging of hematopoietic stem cells: DNA damage and mutations? *Exp Hematol* **44**, 895-901, doi:10.1016/j.exphem.2016.06.253 (2016).
22 Mansell, E. *et al.* Mitochondrial Potentiation Ameliorates Age-Related Heterogeneity in Hematopoietic Stem Cell Function. *Cell Stem Cell* **28**, 241-256.e246, doi:10.1016/j.stem.2020.09.018 (2021).
23 Florian, M. C. *et al.* Cdc42 activity regulates hematopoietic stem cell aging and rejuvenation. *Cell Stem Cell* **10**, 520-530, doi:10.1016/j.stem.2012.04.007 (2012).
24 Florian, M. C. *et al.* Aging alters the epigenetic asymmetry of HSC division. *PLoS Biol* **16**, e2003389, doi:10.1371/journal.pbio.2003389 (2018).
25 Mejia-Ramirez, E. & Florian, M. C. Understanding intrinsic hematopoietic stem cell aging. *Haematologica* **105**, 22-37, doi:10.3324/haematol.2018.211342 (2020).
26 Sun, D. *et al.* Epigenomic profiling of young and aged HSCs reveals concerted changes during aging that reinforce self-renewal. *Cell Stem Cell* **14**, 673-688, doi:10.1016/j.stem.2014.03.002 (2014).
27 Beerman, I., Seita, J., Inlay, M. A., Weissman, I. L. & Rossi, D. J. Quiescent hematopoietic stem cells accumulate DNA damage during aging that is repaired upon entry into cell cycle. *Cell Stem Cell* **15**, 37-50, doi:10.1016/j.stem.2014.04.016 (2014).
28 Chen, X. *et al.* Bone Marrow Myeloid Cells Regulate Myeloid-Biased Hematopoietic Stem Cells via a Histamine-Dependent Feedback Loop. *Cell Stem Cell* **21**, 747-760.e747, doi:10.1016/j.stem.2017.11.003 (2017).
29 Pinho, S. *et al.* Lineage-Biased Hematopoietic Stem Cells Are Regulated by Distinct Niches. *Dev Cell* **44**, 634-641.e634, doi:10.1016/j.devcel.2018.01.016 (2018).
30 Morita, Y., Ema, H. & Nakauchi, H. Heterogeneity and hierarchy within the most primitive hematopoietic stem cell compartment. *J Exp Med* **207**, 1173-1182, doi:10.1084/jem.20091318 (2010).
31 Kim, K. M. *et al.* Taz protects hematopoietic stem cells from an aging-dependent decrease in PU.1 activity. *Nat Commun* **13**, 5187, doi:10.1038/s41467-022-32970-1 (2022).
32 Beerman, I. *et al.* Functionally distinct hematopoietic stem cells modulate hematopoietic lineage potential during aging by a mechanism of clonal expansion. *Proc Natl Acad Sci U S A* **107**, 5465-5470, doi:10.1073/pnas.1000834107 (2010).
33 Gulati, G. S. *et al.* Neogenin-1 distinguishes between myeloid-biased and balanced Hoxb5 (+) mouse long-term hematopoietic stem cells. *Proc Natl Acad Sci U S A* **116**, 25115-25125, doi:10.1073/pnas.1911024116 (2019).
34 Montecino-Rodriguez, E. *et al.* Lymphoid-Biased Hematopoietic Stem Cells Are Maintained with Age and Efficiently Generate Lymphoid Progeny. *Stem Cell Reports* **12**, 584-596, doi:10.1016/j.stemcr.2019.01.016 (2019).
35 Liang, R. *et al.* Restraining Lysosomal Activity Preserves Hematopoietic Stem Cell Quiescence and Potency. *Cell Stem Cell* **26**, 359-376.e357, doi:10.1016/j.stem.2020.01.013 (2020).

36 Challen, G. A., Boles, N. C., Chambers, S. M. & Goodell, M. A. Distinct hematopoietic stem cell subtypes are differentially regulated by TGF-beta1. *Cell Stem Cell* **6**, 265-278, doi:10.1016/j.stem.2010.02.002 (2010).
37 Foudi, A. *et al.* Analysis of histone 2B-GFP retention reveals slowly cycling hematopoietic stem cells. *Nat Biotechnol* **27**, 84-90, doi:10.1038/nbt.1517 (2009).
38 Qiu, J., Papatsenko, D., Niu, X., Schaniel, C. & Moore, K. Divisional history and hematopoietic stem cell function during homeostasis. *Stem Cell Reports* **2**, 473-490, doi:10.1016/j.stemcr.2014.01.016 (2014).
39 Bernitz, J. M., Kim, H. S., MacArthur, B., Sieburg, H. & Moore, K. Hematopoietic Stem Cells Count and Remember Self-Renewal Divisions. *Cell* **167**, 1296-1309.e1210, doi:10.1016/j.cell.2016.10.022 (2016).
40 Morrison, S. J., Wandycz, A. M., Akashi, K., Globerson, A. & Weissman, I. L. The aging of hematopoietic stem cells. *Nature Medicine* **2**, 1011-1016, doi:10.1038/nm0996-1011 (1996).
41 Kuribayashi, W. *et al.* Limited rejuvenation of aged hematopoietic stem cells in young bone marrow niche. *J Exp Med* **218**, doi:10.1084/jem.20192283 (2021).
42 Hao, T. *et al.* An aging mouse model of human chronic myeloid leukemia. *Oncogene* **40**, 3152-3163, doi:10.1038/s41388-021-01770-0 (2021).
43 Cossarizza, A. *et al.* CD45 isoforms expression on CD4+ and CD8+ T cells throughout life, from newborns to centenarians: implications for T cell memory. *Mech Ageing Dev* **86**, 173-195, doi:10.1016/0047-6374(95)01691-0 (1996).
44 van der Geest, K. S. *et al.* Aging disturbs the balance between effector and regulatory CD4+ T cells. *Exp Gerontol* **60**, 190-196, doi:10.1016/j.exger.2014.11.005 (2014).
45 Horvath, S. & Raj, K. DNA methylation-based biomarkers and the epigenetic clock theory of ageing. *Nat Rev Genet* **19**, 371-384, doi:10.1038/s41576-018-0004-3 (2018).
46 Flohr Svendsen, A. *et al.* A comprehensive transcriptome signature of murine hematopoietic stem cell aging. *Blood* **138**, 439-451, doi:10.1182/blood.2020009729 (2021).
47 Booth, L. N. & Brunet, A. The Aging Epigenome. *Mol Cell* **62**, 728-744, doi:10.1016/j.molcel.2016.05.013 (2016).
48 Pal, S. & Tyler, J. K. Epigenetics and aging. *Sci Adv* **2**, e1600584, doi:10.1126/sciadv.1600584 (2016).
49 Sen, P., Shah, P. P., Nativio, R. & Berger, S. L. Epigenetic Mechanisms of Longevity and Aging. *Cell* **166**, 822-839, doi:10.1016/j.cell.2016.07.050 (2016).
50 Itokawa, N. *et al.* Epigenetic traits inscribed in chromatin accessibility in aged hematopoietic stem cells. *Nat Commun* **13**, 2691, doi:10.1038/s41467-022-30440-2 (2022).
51 Shcherbina, A. *et al.* Dissecting Murine Muscle Stem Cell Aging through Regeneration Using Integrative Genomic Analysis. *Cell Rep* **32**, 107964, doi:10.1016/j.celrep.2020.107964 (2020).
52 Wang, J. *et al.* ATAC-Seq analysis reveals a widespread decrease of chromatin accessibility in age-related macular degeneration. *Nat Commun* **9**, 1364, doi:10.1038/s41467-018-03856-y (2018).
53 Beerman, I. Accumulation of DNA damage in the aged hematopoietic stem cell compartment. *Semin Hematol* **54**, 12-18, doi:10.1053/j.seminhematol.2016.11.001 (2017).

54 Li, T., Zhou, Z. W., Ju, Z. & Wang, Z. Q. DNA Damage Response in Hematopoietic Stem Cell Ageing. *Genomics Proteomics Bioinformatics* **14**, 147-154, doi:10.1016/j.gpb.2016.04.002 (2016).
55 Rodriguez-Fraticelli, A. E. *et al.* Clonal analysis of lineage fate in native haematopoiesis. *Nature* **553**, 212-216, doi:10.1038/nature25168 (2018).
56 Kiel, M. J. *et al.* SLAM family receptors distinguish hematopoietic stem and progenitor cells and reveal endothelial niches for stem cells. *Cell* **121**, 1109-1121, doi:10.1016/j.cell.2005.05.026 (2005).
57 Young, K. *et al.* Decline in IGF1 in the bone marrow microenvironment initiates hematopoietic stem cell aging. *Cell Stem Cell* **28**, 1473-1482.e1477, doi:10.1016/j.stem.2021.03.017 (2021).
58 Wendorff, A. A. *et al.* Epigenetic reversal of hematopoietic stem cell aging in Phf6-knockout mice. *Nat Aging* **2**, 1008-1023, doi:10.1038/s43587-022-00304-x (2022).
59 Ergen, A. V., Boles, N. C. & Goodell, M. A. Rantes/Ccl5 influences hematopoietic stem cell subtypes and causes myeloid skewing. *Blood* **119**, 2500-2509, doi:10.1182/blood-2011-11-391730 (2012).
60 Ocampo, A. *et al.* In Vivo Amelioration of Age-Associated Hallmarks by Partial Reprogramming. *Cell* **167**, 1719-1733.e1712, doi:10.1016/j.cell.2016.11.052 (2016).
61 Browder, K. C. *et al.* In vivo partial reprogramming alters age-associated molecular changes during physiological aging in mice. *Nat Aging* **2**, 243-253, doi:10.1038/s43587-022-00183-2 (2022).
62 Lu, Y. *et al.* Reprogramming to recover youthful epigenetic information and restore vision. *Nature* **588**, 124-129, doi:10.1038/s41586-020-2975-4 (2020).
63 Schroer, A. B. *et al.* Platelet factors attenuate inflammation and rescue cognition in ageing. *Nature* **620**, 1071-1079, doi:10.1038/s41586-023-06436-3 (2023).
64 Smith, S. C. *et al.* GDF11 does not rescue aging-related pathological hypertrophy. *Circ Res* **117**, 926-932, doi:10.1161/circresaha.115.307527 (2015).
65 Egerman, M. A. *et al.* GDF11 Increases with Age and Inhibits Skeletal Muscle Regeneration. *Cell Metab* **22**, 164-174, doi:10.1016/j.cmet.2015.05.010 (2015).
66 Ross, J. B. *et al.* Depleting myeloid-biased haematopoietic stem cells rejuvenates aged immunity. *Nature* **628**, 162-170, doi:10.1038/s41586-024-07238-x (2024).
67 Szade, K., Bukowska-Strakova, K., Zukowska, M., Jozkowicz, A. & Dulak, J. Analysis of Cell Cycle Status of Murine Hematopoietic Stem Cells. *Methods Mol Biol* **1516**, 91-99, doi:10.1007/7651_2016_361 (2016).
68 Picelli, S. *et al.* Smart-seq2 for sensitive full-length transcriptome profiling in single cells. *Nat Methods* **10**, 1096-1098, doi:10.1038/nmeth.2639 (2013).
69 Chen, R. *et al.* Decoding molecular and cellular heterogeneity of mouse nucleus accumbens. *Nat Neurosci* **24**, 1757-1771, doi:10.1038/s41593-021-00938-x (2021).
70 Pakpour, N., Zaph, C. & Scott, P. The central memory CD4+ T cell population generated during Leishmania major infection requires IL-12 to produce IFN-gamma. *J Immunol* **180**, 8299-8305, doi:10.4049/jimmunol.180.12.8299 (2008).
71 Dougherty, J. P., Springer, D. A. & Gershengorn, M. C. The Treadmill Fatigue Test: A Simple, High-throughput Assay of Fatigue-like Behavior for the Mouse. *J Vis Exp*, doi:10.3791/54052 (2016).
72 Chen, R. *et al.* Cell type-specific mechanism of Setd1a heterozygosity in schizophrenia pathogenesis. *Sci Adv* **8**, eabm1077, doi:10.1126/sciadv.abm1077 (2022).

73 Kim, D., Langmead, B. & Salzberg, S. L. HISAT: a fast spliced aligner with low memory requirements. *Nat Methods* **12**, 357-360, doi:10.1038/nmeth.3317 (2015).
74 Danecek, P. *et al.* Twelve years of SAMtools and BCFtools. *Gigascience* **10**, doi:10.1093/gigascience/giab008 (2021).
75 Anders, S., Pyl, P. T. & Huber, W. HTSeq--a Python framework to work with high-throughput sequencing data. *Bioinformatics* **31**, 166-169, doi:10.1093/bioinformatics/btu638 (2015).
76 Love, M. I., Huber, W. & Anders, S. Moderated estimation of fold change and dispersion for RNA-seq data with DESeq2. *Genome Biol* **15**, 550, doi:10.1186/s13059-014-0550-8 (2014).
77 Zhang, Y. *et al.* Model-based analysis of ChIP-Seq (MACS). *Genome Biol* **9**, R137, doi:10.1186/gb-2008-9-9-r137 (2008).
78 Ross-Innes, C. S. *et al.* Differential oestrogen receptor binding is associated with clinical outcome in breast cancer. *Nature* **481**, 389-393, doi:10.1038/nature10730 (2012).
79 Ramírez, F. *et al.* deepTools2: a next generation web server for deep-sequencing data analysis. *Nucleic Acids Res* **44**, W160-165, doi:10.1093/nar/gkw257 (2016).
80 Hao, Y. *et al.* Integrated analysis of multimodal single-cell data. *Cell* **184**, 3573-3587.e3529, doi:10.1016/j.cell.2021.04.048 (2021).
81 Krueger, F. & Andrews, S. R. Bismark: a flexible aligner and methylation caller for Bisulfite-Seq applications. *Bioinformatics* **27**, 1571-1572, doi:10.1093/bioinformatics/btr167 (2011).
82 Meer, M. V., Podolskiy, D. I., Tyshkovskiy, A. & Gladyshev, V. N. A whole lifespan mouse multi-tissue DNA methylation clock. *Elife* **7**, doi:10.7554/eLife.40675 (2018).

Figure Legends

Fig. 1: Transplantation of young HSCs rejuvenates old mice. a, Diagram illustration of the competitive young (2-3 months) and old (22-24 months) HSC transplantation experiment. For the first transplantation, the ratio of young to old HSCs was 1:2 (500 young and 1,000 old) while the ratio was 1:1 (1,000 young and 1,000 old) for the second transplantation. **b,** Peripheral blood chimerism of donor HSCs at different times after the 1st and 2nd transplantation. n=6 for the first and n=3 for the second transplantation. **c,** Diagram showing the experimental design of individual transplantation of 1,000 young (3 months) or 1,000 old (22-24 months) HSCs into middle-aged recipients (13-month-old). Five months after the transplantation, a series of hematopoietic and physical tests were performed. **d,** Bar graph showing the percentage of B, T and myeloid cells in the peripheral blood (PB) of recipient mice, n=8. **e,** Bar graph showing the absolute number of blood cells in the PB of recipient mice, n=8. **f,** FACS plot and bar plot showing the percentage of naïve T cells in CD8+ T cells from recipient mice, Naïve T cells ($CD44^{low}$, $CD62L^{high}$), Tcm ($CD44^{high}$, $CD62L^{high}$) and Tem ($CD44^{high}$, $CD62L^{low}$), n=8. **g,** Bar plot showing the epigenetic age of blood from recipient mice, n=4. **h,** Physical tests of recipient mice that received young or old HSCs. Muscle strength, motor coordination, endurance and brain function were assessed, n=8.
Mean ± SD, student t test, *$p<0.05$, **$p<0.01$, ****$p<0.0001$.

Fig. 2: scRNA-seq reveals increased heterogeneity of old HSCs. a, Workflow of 10X scRNA-seq of young and old HSCs. The HSCs were sorted from young (2-3 months) and old (23 months) mice. **b,** UMAP plot showing the distribution of young and old HSCs based on scRNA-seq. Clear separation of young and old HSCs indicates transcriptional changes of HSCs during aging. **c,** Cell cycle phase analysis of young and old HSCs based on scRNA-seq. The S-phase and G2/M-phase marker genes are from Seurat package (V4.0.2). The cell cycle phase is determined by the relative expression levels of these marker genes. If neither S-phase nor G2/M phase genes are expressed, they are classified as G0/G1 phase. **d,** UMAP plot showing unsupervised clustering of young and old HSCs. In total, 6 clusters were identified with two clusters (a1 and a2) representing active, and four clusters (q1-q4) representing quiescent cells. **e,** Heatmap showing the cluster-specific marker genes expression across the 6 clusters and their

enriched GO terms. Differentially expressed genes with min.pct = 0.25, logfc.threshold = 0.25 among the 6 clusters were used to generate the heatmap. Well-known HSC aging related genes in clusters q1 and q2 are highlighted. Commonly identified marker genes in clusters q3 and q4 were also highlighted. **f,** Box plot showing relative expression of marker genes of q1, q2 and q3 in young and old HSCs via analysis of bulk RNA-seq. The expression level was normalized to the average expression level of the old. Plot shows the mean and 5-95 percentile. Two-sided unpaired Wilcoxon test. **g,** UMAP presentation of well-known HSC aging marker genes, *Sbspon*, *Gpr183*, *Clu* and *Ramp2* in each of the single cells. **h,** UMAP plot and violin plot showing the calculated aging score of single cells of different clusters based on the HSC aging genes identified in bulk RNA-seq. In total, 332 up-regulated genes in old HSCs were used for aging score calculation. Two-sided unpaired Wilcoxon test. **p<0.01, ****p<0.0001.

Fig. 3: Identification of CD150 as a HSC aging heterogeneity marker. a, Workflow for identifying heterogeneity marker genes in old HSCs. **b,** FACS plot showing expression level of CD150 in young (3 months) and old (22-24 months) HSCs. **c,** HSCs from old mice were separated into four subgroups (25% for each) based on their CD150 protein levels and subjected to bulk RNA-seq, n=3. **d,** Dot plot showing Pearson correlation between CD150 signature score and aging score based on scRNA-seq data, R=0.78. **e,** Heatmap showing changes in expression of aging-related genes with ascending level of CD150 based on bulk RNA-seq in (C). **f,** Bar plot showing the epigenetic age of $CD150^{low}$ and $CD150^{high}$ HSCs from 22-24 months old mice, n=4, paired t test, the HSC subsets from the same mice were paired with dash line. **g,** Line plot and heatmap showing ATAC-seq signal difference between $CD150^{low}$ and $CD150^{high}$ HSCs in aging-related open and closed regions, respectively. **h,** Diagram of competitive transplantation to evaluate the repopulation capacity of $CD150^{low}$ and $CD150^{high}$ HSCs from old mice. **i,** Whole blood chimerism of $CD150^{low}$ and $CD150^{high}$ HSCs from 22-24 months old donor mice at different time after the 1st and 2nd transplantation. n=6 for the first and n=3 for the second transplantation.

Mean ± SD, student t test, *p<0.05, **p<0.01, ****p<0.0001.

Fig. 4: Differentiation, but not self-renewal, is a major defect of old $CD150^{high}$ HSCs. a, Diagram illustration of the transplantation experiment comparing old $CD150^{low}$ and $CD150^{high}$

HSCs. Donor HSCs derived HSPCs from the bone marrow were analyzed on days 7 and 14 after transplantation. **b,** Representative FACS analysis of donor HSCs derived HSPCs (left) and quantification of different cell populations 7 days after transplantation (right). LT-HSC (CD45.2 LSK, $CD34^{-}CD48^{-}CD150^{+}$), ST-HSC (CD45.2 LSK, $CD34^{+}/CD48^{+}CD150^{+}$) and MPPs (CD45.2 LSK, $CD34^{+}/CD48^{+}CD150^{-}$) were analyzed, n=3. **c,** Diagram illustration of the competitive transplantation for evaluating the long-term differentiation of $CD150^{high}$ HSCs. Both peripheral blood and bone marrow were analyzed five months after transplantation. **d,** Representative FACS analysis of donor HSC-derived HSPCs (left) and quantification of different cell populations (right) 5 months after transplantation, n=3. **e,** Bar graph showing the chimerism of donor HSCs in LT-HSCs, ST-HSCs, MPPs and PB 5 months after transplantation, n=3. **f,** UMAP plot showing cell distribution of HSPCs derived from $CD150^{low}$ and $CD150^{high}$ HSCs in scRNA-seq 14 days after transplantation. **g,** UMAP presentation of cell types predicted based on HSPC marker gene expression (left). In total, 7 different cell types were identified in HSPCs. **h,** Bar graph showing relative abundance of predicted cell types in HSPCs from mice that received old $CD150^{low}$ or $CD150^{high}$ HSCs. Mean ± SD, student t test, *p<0.05, **p<0.01, ***p<0.001.

Fig. 5: Transplantation of "youthful" subset old HSCs alleviates aging phenotypes of aged mice. a, Diagram showing the experiment design of individual transplantation of 2,000 old $CD150^{low}$ (25% lowest), whole-HSCs (un-selected) and $CD150^{high}$ (25% highest) HSCs into middle-aged recipients (13-month-old), n=8. Five months after transplantation, a series of hematopoietic and physical tests were performed. **b,** Bar graph showing the percentage of B, T and myeloid cells in the PB of recipient mice of the three groups, n=8. **c,** Bar graph showing absolute number of blood cells in PB of recipient mice from different transplanted groups, n=8. **d,** Representative FACS analysis of naïve T cells, central memory T cells (Tcm) and effector T cells (Tem) ratio in CD8 positive T cells and their quantification in recipient mice of the three groups, n=8. **e,** Physical tests of recipient mice that received $CD150^{low}$, whole-HSCs and $CD150^{high}$ HSCs. Muscle strength, motor coordination and endurance were assessed, n=8. **f,** Bar graph showing the epigenetic age of recipient mice from different groups, n=4. **g,** Survival curve showing the lifespan difference among recipient mice that received old $CD150^{low}$, whole-HSCs and $CD150^{high}$ HSCs, each mice received 2,000 HSCs. Log-rank (Mantel-Cox) test, n=17. For (**b-f**), Mean ± SD, one-way ANOVA, *p<0.05, **p<0.01, ***p<0.001, ****p<0.0001.

Fig. 6: Reducing dysfunctional HSCs ameliorates aging phenotypes in old mice after transplantation. **a,** Diagram showing the experiment design. Individual transplantation of 500 old CD150^{low} HSCs with: 2,500 CD150^{high} HSCs (1:5 group); 1,000 CD150^{high} HSCs (1:2 group) and 0 CD150^{high} HSCs (1:0 group) into middle-aged recipients (13-months-old). Five months after transplantation, a series hematopoietic and physical tests were performed. **b,** Bar graph showing the percentage of B, T and myeloid cells in the PB of recipient mice of the different groups. **c,** Bar graph showing absolute number of blood cells in PB of recipient mice from different transplanted groups. **d,** Representative FACS analysis of naïve T cells and effector T cells (Tem) ratio in CD8 positive T cells and their quantification in recipient mice of different groups. **e,** Bar plot showing the results of physical functional tests of recipient mice of different groups. Muscle strength, motor coordination, endurance and locomotor activity were assessed. n=6 for 1:5 and 1:2 group, n=7 for 1:0 group, Mean ± SD, one-way ANOVA, *p<0.05, **p<0.01.

Extended Data Figure Legends

Extended Data Fig. 1: Aging-related functional decline of HSCs in mouse (related to Fig. 1). a. The gating strategy for LT-HSCs sorting. The lineage^{-}Sca-1^{+}c-Kit^{+}(LSK) was first gated, and LT-HSCs (CD48^{-}CD34^{-}CD150^{+}) were gated in LSK population. **b.** Bar graph showing the percentage of LT-HSCs in LSK HSPCs from young (2-3 months) and old (22-24 months) mice, n=10 for young, n=9 for old. **c-d.** Peripheral blood chimerism of donor HSCs at different time after the first (c) and second (d) transplantation, n=6 for the first and n=3 for the second transplantation. **e.** Diagram illustration of individual transplantation of young and old HSCs into young recipient mice for assessing differentiation bias. **f.** Analysis of HSCs differentiation toward T, B and myeloid cells at different time after transplantation, n=3. Mean ± SD, student t test, *p<0.05, **p<0.01, ***p<0.001, ****p<0.0001.

Extended Data Fig. 2: Immune profile alterations during aging in mice (related to Fig. 1).

(**a-b**) Representative FACS analysis and bar plot showing the change in percentage of naïve, Tcm and Tem with aging in PB of mouse in CD8+ T cells (a) and CD4+ T cells (b). Mean ± SD, student t test, n=4, *p<0.05, **p<0.01, ***p<0.001, ****p<0.0001.

Extended Data Fig. 3: Transplantation of young HSCs rejuvenates old mice (related to Fig. 1). a. Representative FACS analysis and bar plot showing the percentage of naïve T cells in CD4+ T cells from recipient mice, n=8. **b.** Bar plot showing the body weight of recipient mice that received young or old HSCs, n=8. **c.** Bar plot showing the total moving distance and the ratio of duration in novel arm to familiar arm in Y maze test of recipient mice, n=8. **d.** Bar plot showing the results of fear conditioning test. Compared to acclimation, the increased freezing time was calculated, n=8. Mean ± SD, student t test, **p<0.01, ns, not significant.

Extended Data Fig. 4: scRNA-seq reveals increased heterogeneity of old HSCs (related to Fig. 2). a. Heatmap showing HSC aging related genes that were identified through bulk RNA-seq analysis. Well-known HSC marker genes in public datasets were highlighted. **b.** Bar graph showing the enriched GO terms in HSC aging related up and down genes identified in (a). **c.** UMAP showing the expression of the young HSC marker genes (*Rnase6* and *Arhgap30*) in single cells. **d.** UMAP (left) showing the calculated aging score based on public HSC aging marker genes (Supplementary Table 3) in each single cell. Violin plot (right) showing the aging score of cells from different clusters. Two-sided unpaired Wilcoxon test, **** p<0.0001.

Extended Data Fig. 5: CD150 can serve as an aging heterogeneity marker of old HSCs (related to Fig. 3). a. Dot plot showing ranking of genes based on the correlation of their expression and aging score in scRNA-seq. The top 150 highly ranked genes were highlighted. **b.** Violin plot showing expression level of potential marker genes in cluster q1, q2 and q3 by scRNA-seq. **c.** Dot plot showing the ranking of genes based on their correlation with CD150 levels in expression of the four cell groups in Figure 3C measured by bulk RNA-seq. A total of 131 positively correlated genes (R>0.8) and 103 negatively correlated genes (R<-0.75) were identified as CD150 related genes. **d.** Heatmap showing expression changes of CD150-related genes with ascending CD150 level based on bulk RNA-seq. For positive correlated genes, previously identified HSC aging marker genes are highlighted. For negative correlated genes,

genes that are highly expressed in young HSCs are highlighted. **e-f.** Feature plot (e) and violin plot (f) showing CD150 signature scores of the six cell clusters in scRNA-seq. **g.** Representative images and bar plot showing the level of γH2AX in old CD150^{low} and CD150^{high} HSCs, n=3. **h.** Left, representative FACS plot showing the percentage of old CD150^{low} and CD150^{high} HSCs in different cell cycle phases. Right, bar graph showing the percentage of old CD150^{low} and CD150^{high} HSCs in active cell cycle (G1 and G2/S/M), n=3. For (g) and (h), Mean ± SD, student t test, *p<0.05, **p<0.01. For (f), Two-sided unpaired Wilcoxon test, ****p<0.0001.

Extended Data Fig. 6: Old CD150^{low} HSCs are functionally superior to CD150^{high} HSCs *in vivo* (related to Fig. 3). a-b. The peripheral blood chimerism of donor HSCs at different time after transplantation in the first (a) and second (b) competitive transplantation. B, T, and myeloid cells were analyzed individually. Mean ± SD, student t test, n=6 for the first and n=3 for the second transplantation, *p<0.05, **p<0.01, ****p<0.0001.

Extended Data Fig. 7: Comparable function of CD150^{low} and CD150^{high} HSCs from young mice (related to Fig. 3). a. Left, representative FACS plot showing the percentage of young CD150^{low} (25% lowest) and CD150^{high} (25% highest) HSCs in different cell cycle phases. Right, bar graph showing the average percentage of young CD150^{low} and CD150^{high} HSCs in active cell cycle (G1 and G2/S/M), n=3. **b.** Diagram illustrating the competitive transplantation for evaluating the repopulating capacity of CD150^{low} and CD150^{high} HSCs from young mice. The ratio of competitor to donor HSCs to was 1:2 (300 competitor HSCs with 600 donor HSCs). **c.** The peripheral blood chimerism of donor HSCs at different time after transplantation. Whole blood, T, B, and myeloid cells were analyzed. n=3, Mean ± SD, student t test, *p<0.05, **p<0.01, ns, not significant.

Extended Data Fig. 8: Differentiation, but not self-renewal, is a major defect of old CD150^{high} HSCs (related to Fig. 4). a. Diagram of individual transplantation of old HSCs to study the differentiation trajectory after transplantation. The donor HSCs derived HSPCs in bone

marrow were analyzed on days 4, 7, 10 and 14 after transplantation. **b.** FACS analysis showing the differentiation trajectory of old HSCs after transplantation. On the 4th day, most donor HSCs are still maintained as LT-HSCs. From 7th days the LT-HSCs started to differentiate toward MPPs. **c.** Representative FACS analysis of donor HSCs derived HSPCs (left) and quantification of different cell populations after transplantation (right) on day 14, n=3. **d.** Diagram of transplantation to evaluate the difference in activation between old $CD150^{low}$ and $CD150^{high}$ HSCs on day 4 after transplantation. The sorted donor HSCs were collected for transcriptome analysis, n=3. **e.** Venn diagram showing the genes that were commonly activated in old $CD150^{low}$ and $CD150^{high}$ HSCs compared to freshly isolated old $CD150^{low}$ and $CD150^{high}$ HSCs 4 days after transplantation (left). Bar graph showing enriched GO terms of the 794 commonly activated genes (right). **f.** GSEA analysis showing that transplanted HSCs highly express cell cycle related genes in both $CD150^{low}$ (left) and $CD150^{high}$ (right) HSCs when compared with freshly isolated HSCs. **g.** Diagram showing the experimental design for examining HSCs proliferation *in vitro*. In each well, 50 GFP+ cell and 50 old $CD150^{low}$ or $CD150^{high}$ HSCs were co-cultured. The percentage and absolute number of old $CD150^{low}$ and $CD150^{high}$ HSCs were quantified 6 days after culture. **h.** Bar graph showing comparable proliferation rate of old $CD150^{low}$ and $CD150^{high}$ HSCs 6 days after culture. The percentage of non-GFP HSCs was shown, n=10. **i.** Bar graph showing the absolute number of old $CD150^{low}$ and $CD150^{high}$ HSCs 6 days after culture, n=10. **j.** UMAP and bar graph showing the distribution and percentages of cells in different cell cycle phases of HSPCs from $CD150^{low}$ and $CD150^{high}$ HSCs 14 days after transplantation. **k.** Violin plot showing the expression pattern of cell type marker genes, including *Ly6a*, *Kit*, *Cd34*, *Cd48*, *Flt3* and *Slamf1* (CD150). Mean ± SD, student t test, **p<0.01, ***p<0.001, ns, not significant.

Extended Data Fig. 9: Transplantation of "youthful" subset old HSCs attenuates aging phenotypes of old mice (related to Fig. 5).

a. Representative FACS (left) analysis of naïve T cells, Tcm and Tem ratio in CD4 positive T cells of mice from different groups and their quantification (right, bar graphs). **b.** Bar graph showing body weight of recipient mice from different groups. Mean ± SD, one-way ANOVA, n=8, *p<0.05, **p<0.01, ***p<0.001, ns, not significant.

Extended Data Fig. 10: Reducing dysfunctional HSCs ameliorates aging phenotypes in old mice post transplantation (related to Fig. 6). a. Representative FACS (left) analysis of naïve T cells and Tem ratio in CD4 positive T cells of mice from the different groups and their quantification (right, bar graphs). **b.** Bar graph showing body weight of recipient mice from different groups. n=6 for 1:5 and 1:2 group, n=7 for 1:0 group; Mean ± SD, one-way ANOVA, *$p<0.05$, **$p<0.01$, ns, not significant.

Supplementary Tables

Supplementary Table 1: List of DEGs between young and old HSCs derived from bulk RNA-seq

Supplementary Table 2: List of marker genes for the different cell clusters in young and old HSCs generated by scRNA-seq

Supplementary Table 3: List of the top 100 HSC aging marker genes from a public dataset

Supplementary Table 4: List of the 54 potential marker genes for old HSC heterogeneity

Supplementary Table 5: List of the CD150 correlated genes based on bulk RNA-seq

Supplementary Table 6: List of the 794 genes commonly up-regulated in $CD150^{low}$ and $CD150^{high}$ HSCs upon their transplantation

Supplementary Table 7: List of datasets generated in this study

Figure. 1

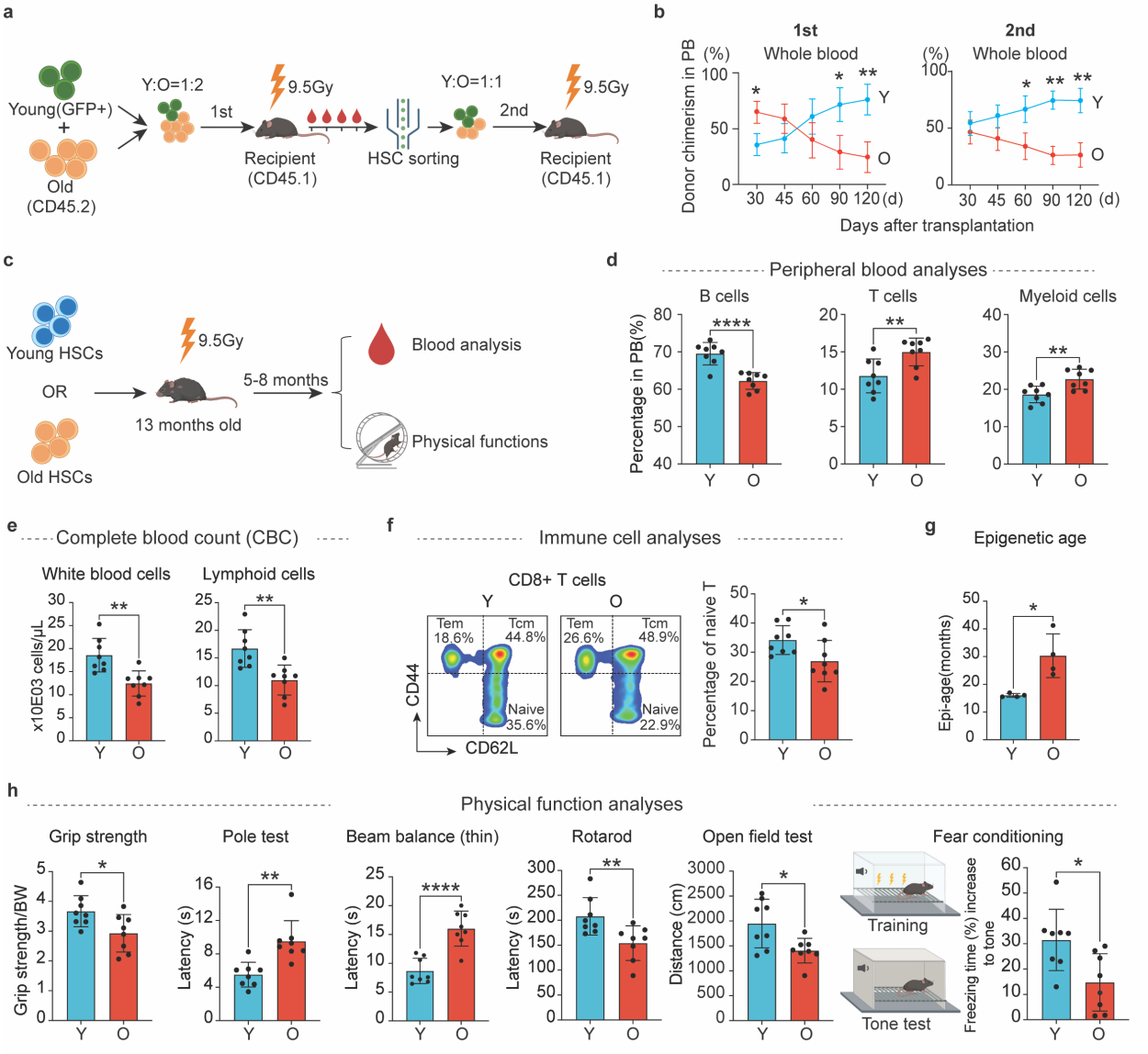
a
Young(GFP+)
+
Old
(CD45.2)
Y:O=1:2
1st
9.5Gy
Recipient
(CD45.1)
HSC sorting
Y:O=1:1
2nd
9.5Gy
Recipient
(CD45.1)
b
1st
Whole blood
2nd
Whole blood
Donor chimerism in PB
(%)
Y
O
Days after transplantation
c
Young HSCs
OR
Old HSCs
9.5Gy
13 months old
5-8 months
Blood analysis
Physical functions
d
Peripheral blood analyses
B cells
T cells
Myeloid cells
Percentage in PB(%)
e
Complete blood count (CBC)
White blood cells
Lymphoid cells
x10E03 cells/μL
f
Immune cell analyses
CD8+ T cells
Tem
Tcm
Naive
CD44
CD62L
Percentage of naive T
g
Epigenetic age
Epi-age(months)
h
Physical function analyses
Grip strength
Pole test
Beam balance (thin)
Rotarod
Open field test
Fear conditioning
Grip strength/BW
Latency (s)
Distance (cm)
Training
Tone test
Freezing time (%) increase to tone

Figure. 2

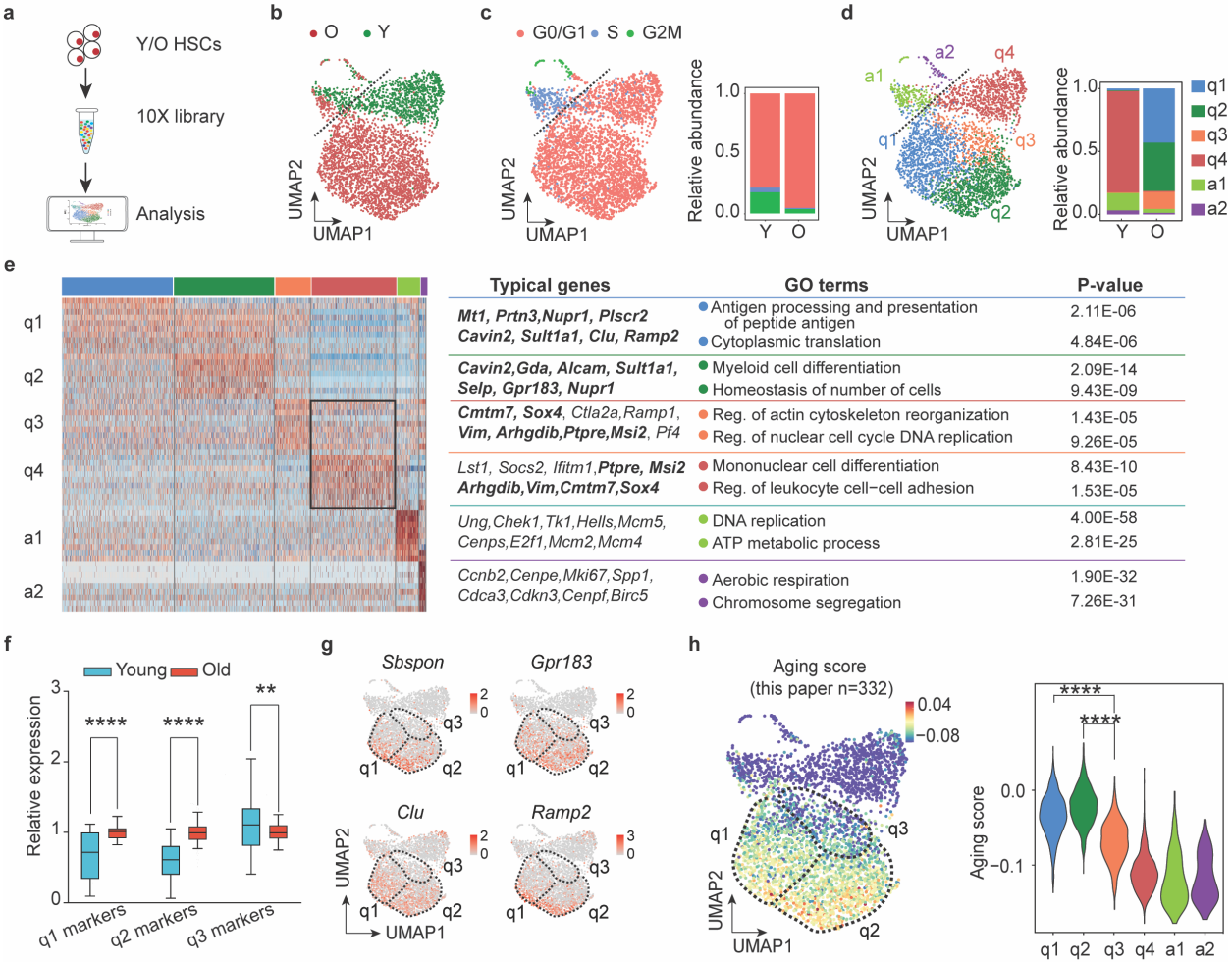
a
Y/O HSCs
10X library
Analysis
b
O
Y
UMAP2
UMAP1
c
G0/G1
S
G2M
UMAP2
UMAP1
Relative abundance
1.0
0.5
0.0
Y
O
d
a2
q4
a1
q1
q3
q2
UMAP2
UMAP1
Relative abundance
1.0
0.5
0.0
Y
O
q1
q2
q3
q4
a1
a2
e
q1
q2
q3
q4
a1
a2
Typical genes
GO terms
P-value
Mt1, Prtn3,Nupr1, Plscr2
Cavin2, Sult1a1, Clu, Ramp2
Antigen processing and presentation of peptide antigen
2.11E-06
Cytoplasmic translation
4.84E-06
Cavin2,Gda, Alcam, Sult1a1,
Selp, Gpr183, Nupr1
Myeloid cell differentiation
2.09E-14
Homeostasis of number of cells
9.43E-09
Cmtm7, Sox4, Ctla2a,Ramp1,
Vim, Arhgdib,Ptpre,Msi2, Pf4
Reg. of actin cytoskeleton reorganization
1.43E-05
Reg. of nuclear cell cycle DNA replication
9.26E-05
Lst1, Socs2, Ifitm1,Ptpre, Msi2
Arhgdib,Vim,Cmtm7,Sox4
Mononuclear cell differentiation
8.43E-10
Reg. of leukocyte cell−cell adhesion
1.53E-05
Ung,Chek1,Tk1,Hells,Mcm5,
Cenps,E2f1,Mcm2,Mcm4
DNA replication
4.00E-58
ATP metabolic process
2.81E-25
Ccnb2,Cenpe,Mki67,Spp1,
Cdca3,Cdkn3,Cenpf,Birc5
Aerobic respiration
1.90E-32
Chromosome segregation
7.26E-31
f
Young
Old
Relative expression
3
2
1
0
****
****
**
q1 markers
q2 markers
q3 markers
g
Sbspon
Gpr183
Clu
Ramp2
q1
q2
q3
UMAP2
UMAP1
h
Aging score
(this paper n=332)
0.04
−0.08
q1
q2
q3
UMAP2
UMAP1
Aging score
0.0
−0.1
****
****
q1
q2
q3
q4
a1
a2

Figure. 3

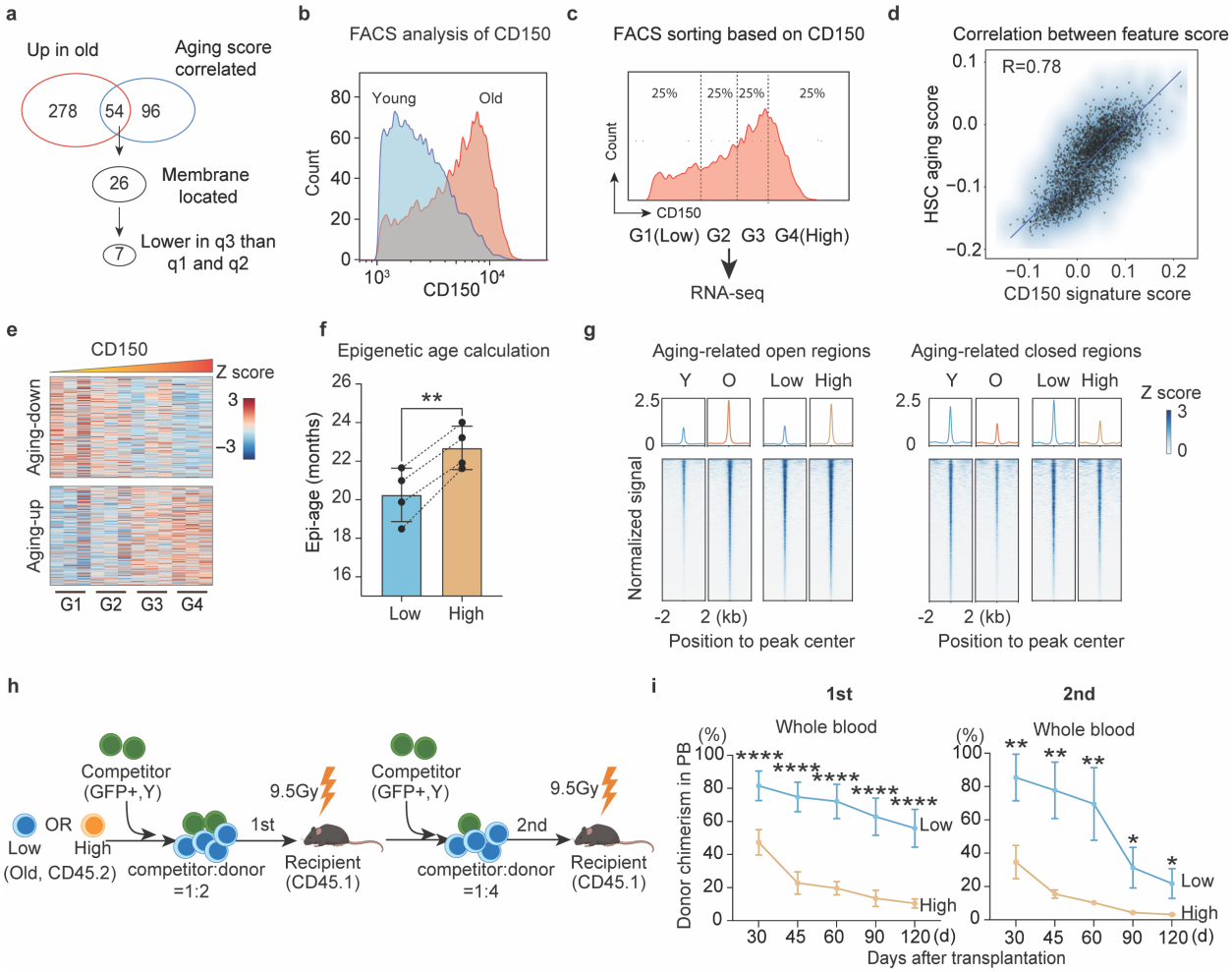
a
Up in old
Aging score correlated
278
54
96
26
Membrane located
7
Lower in q3 than q1 and q2
b
FACS analysis of CD150
Young
Old
Count
CD150
c
FACS sorting based on CD150
25%
Count
CD150
G1(Low) G2 G3 G4(High)
RNA-seq
d
Correlation between feature score
R=0.78
HSC aging score
CD150 signature score
e
CD150
Z score
Aging-down
Aging-up
G1 G2 G3 G4
f
Epigenetic age calculation
Epi-age (months)
Low
High
g
Aging-related open regions
Aging-related closed regions
Y O Low High
Z score
Normalized signal
Position to peak center
h
Competitor (GFP+,Y)
OR
Low
High
(Old, CD45.2)
competitor:donor =1:2
1st
9.5Gy
Recipient (CD45.1)
competitor:donor =1:4
2nd
i
1st
2nd
Whole blood
Donor chimerism in PB
Low
High
Days after transplantation

Figure. 4

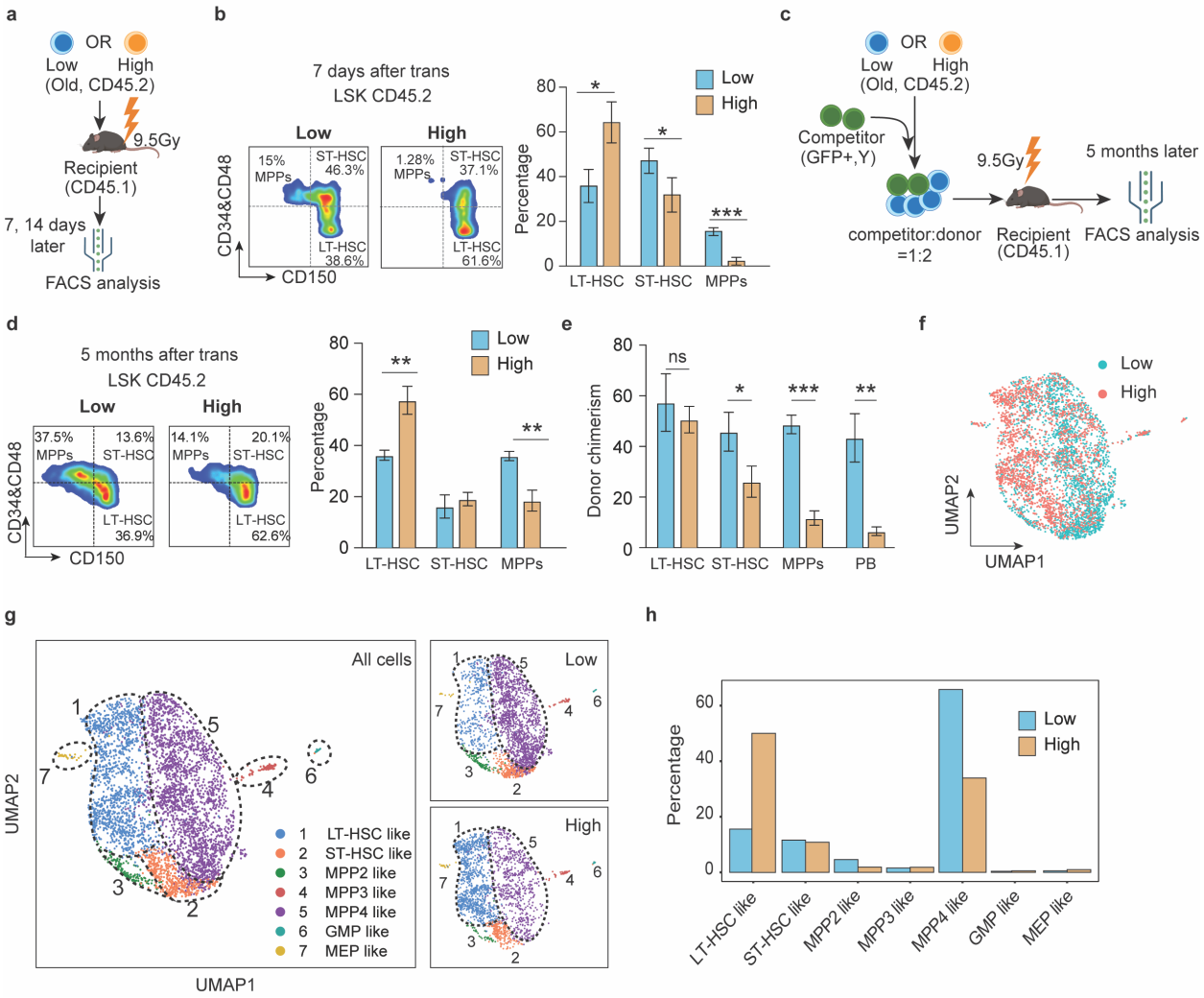
a
OR
Low
High
(Old, CD45.2)
9.5Gy
Recipient
(CD45.1)
7, 14 days
later
FACS analysis
b
7 days after trans
LSK CD45.2
Low
High
15%
MPPs
ST-HSC
46.3%
LT-HSC
38.6%
1.28%
MPPs
ST-HSC
37.1%
LT-HSC
61.6%
CD34&CD48
CD150
Percentage
Low
High
LT-HSC
ST-HSC
MPPs
c
OR
Low
High
(Old, CD45.2)
Competitor
(GFP+,Y)
competitor:donor
=1:2
9.5Gy
Recipient
(CD45.1)
5 months later
FACS analysis
d
5 months after trans
LSK CD45.2
Low
High
37.5%
MPPs
13.6%
ST-HSC
LT-HSC
36.9%
14.1%
MPPs
20.1%
ST-HSC
LT-HSC
62.6%
CD34&CD48
CD150
Percentage
Low
High
LT-HSC
ST-HSC
MPPs
e
Donor chimerism
ns
LT-HSC
ST-HSC
MPPs
PB
f
Low
High
UMAP2
UMAP1
g
All cells
Low
High
1 LT-HSC like
2 ST-HSC like
3 MPP2 like
4 MPP3 like
5 MPP4 like
6 GMP like
7 MEP like
UMAP2
UMAP1
h
Percentage
Low
High
LT-HSC like
ST-HSC like
MPP2 like
MPP3 like
MPP4 like
GMP like
MEP like

Figure. 5

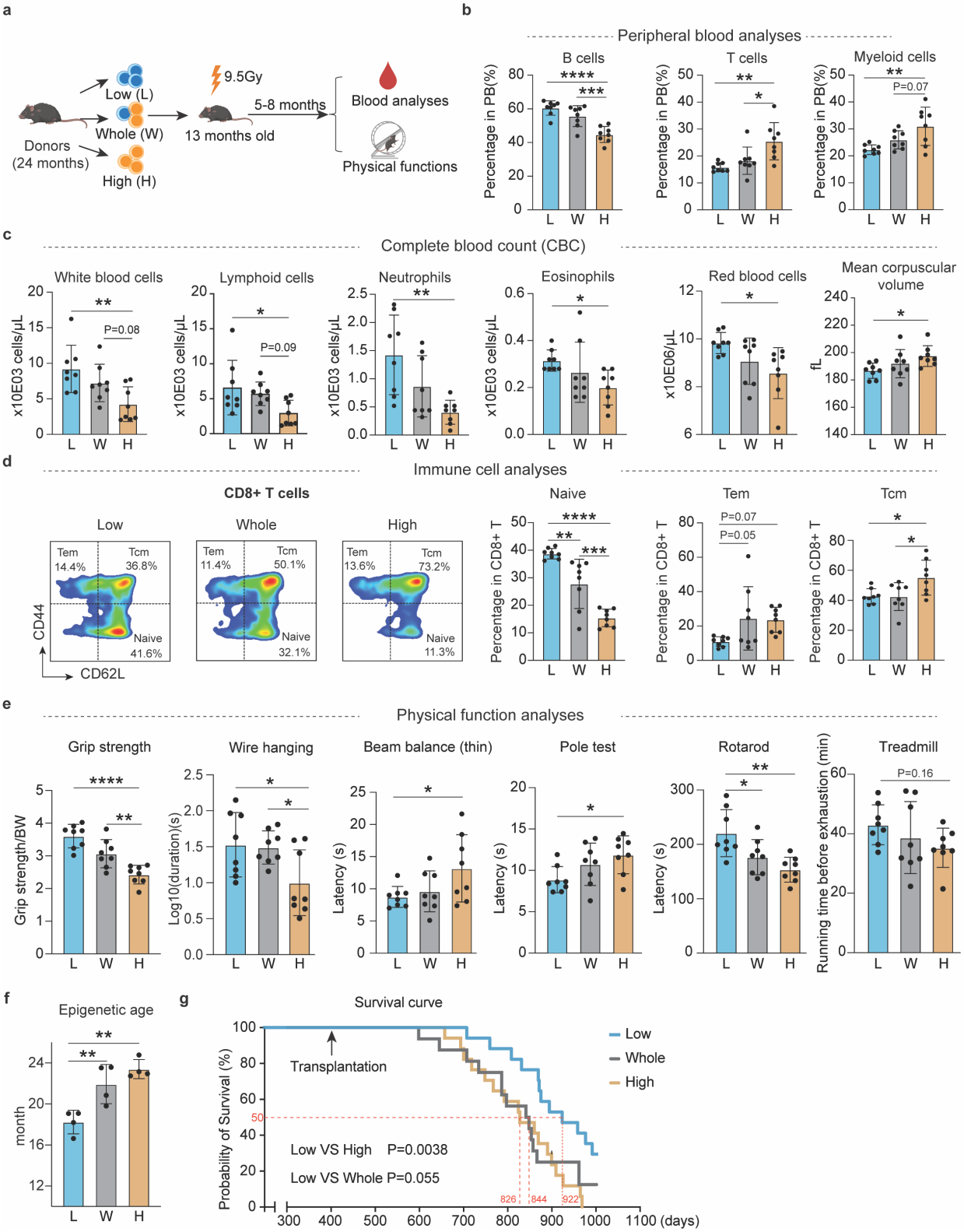
a
Low (L)
Whole (W)
High (H)
Donors
(24 months)
9.5Gy
13 months old
5-8 months
Blood analyses
Physical functions
b
Peripheral blood analyses
B cells
T cells
Myeloid cells
Percentage in PB(%)
P=0.07
c
Complete blood count (CBC)
White blood cells
Lymphoid cells
Neutrophils
Eosinophils
Red blood cells
Mean corpuscular volume
x10E03 cells/μL
x10E06/μL
fL
P=0.08
P=0.09
d
Immune cell analyses
CD8+ T cells
Low
Whole
High
Tem
Tcm
Naive
CD44
CD62L
Percentage in CD8+ T
P=0.07
P=0.05
e
Physical function analyses
Grip strength
Wire hanging
Beam balance (thin)
Pole test
Rotarod
Treadmill
Grip strength/BW
Log10(duration)(s)
Latency (s)
Running time before exhaustion (min)
P=0.16
f
Epigenetic age
month
g
Survival curve
Transplantation
Low
Whole
High
Probability of Survival (%)
Low VS High P=0.0038
Low VS Whole P=0.055
826
844
922
(days)

Figure.6

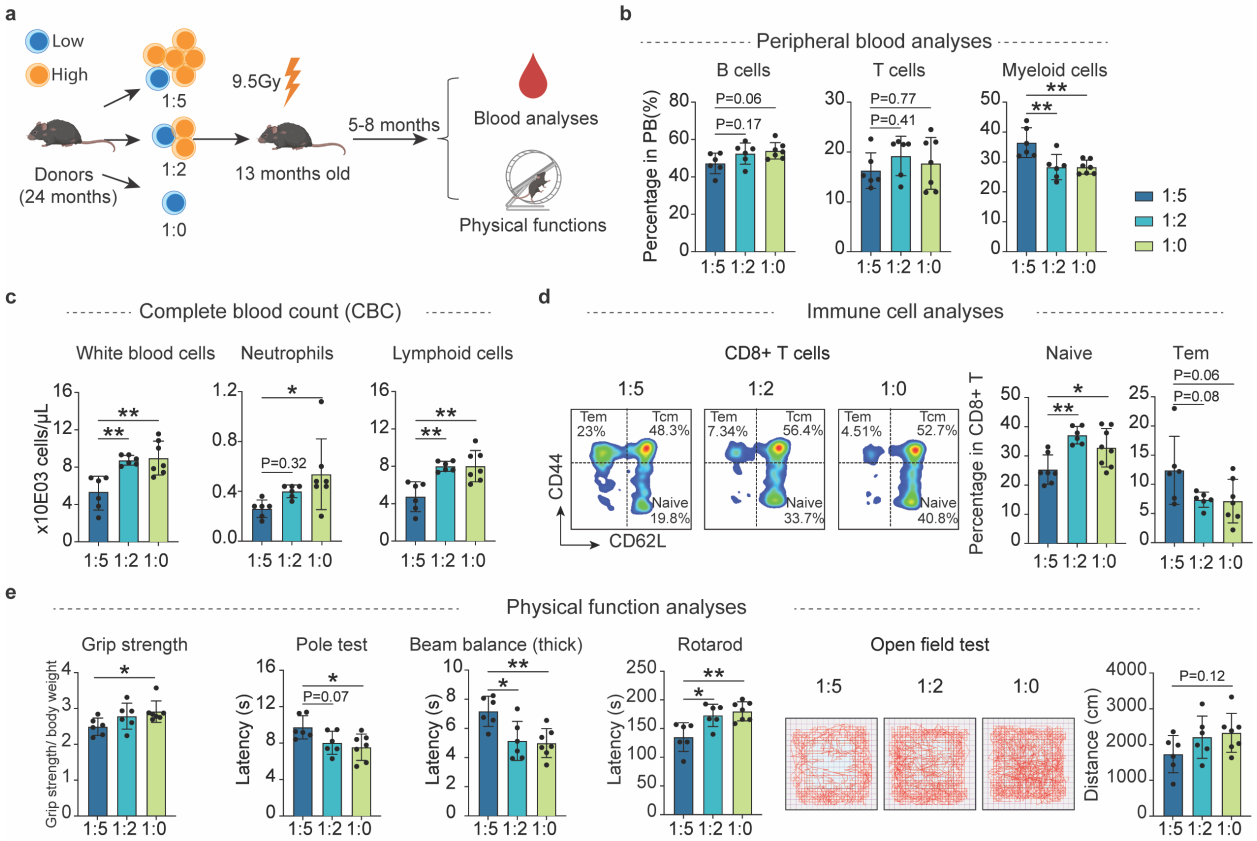
a
Low
High
1:5
1:2
1:0
Donors
(24 months)
9.5Gy
13 months old
5-8 months
Blood analyses
Physical functions
b
Peripheral blood analyses
B cells
T cells
Myeloid cells
Percentage in PB(%)
P=0.06
P=0.17
P=0.77
P=0.41
1:5
1:2
1:0
c
Complete blood count (CBC)
White blood cells
Neutrophils
Lymphoid cells
x10E03 cells/μL
P=0.32
d
Immune cell analyses
CD8+ T cells
Naive
Tem
Tem 23%
Tcm 48.3%
Naive 19.8%
Tem 7.34%
Tcm 56.4%
Naive 33.7%
Tem 4.51%
Tcm 52.7%
Naive 40.8%
CD44
CD62L
Percentage in CD8+ T
P=0.06
P=0.08
e
Physical function analyses
Grip strength
Pole test
Beam balance (thick)
Rotarod
Open field test
Grip strength/ body weight
Latency (s)
P=0.07
Distance (cm)
P=0.12

Extended Data Fig. 1

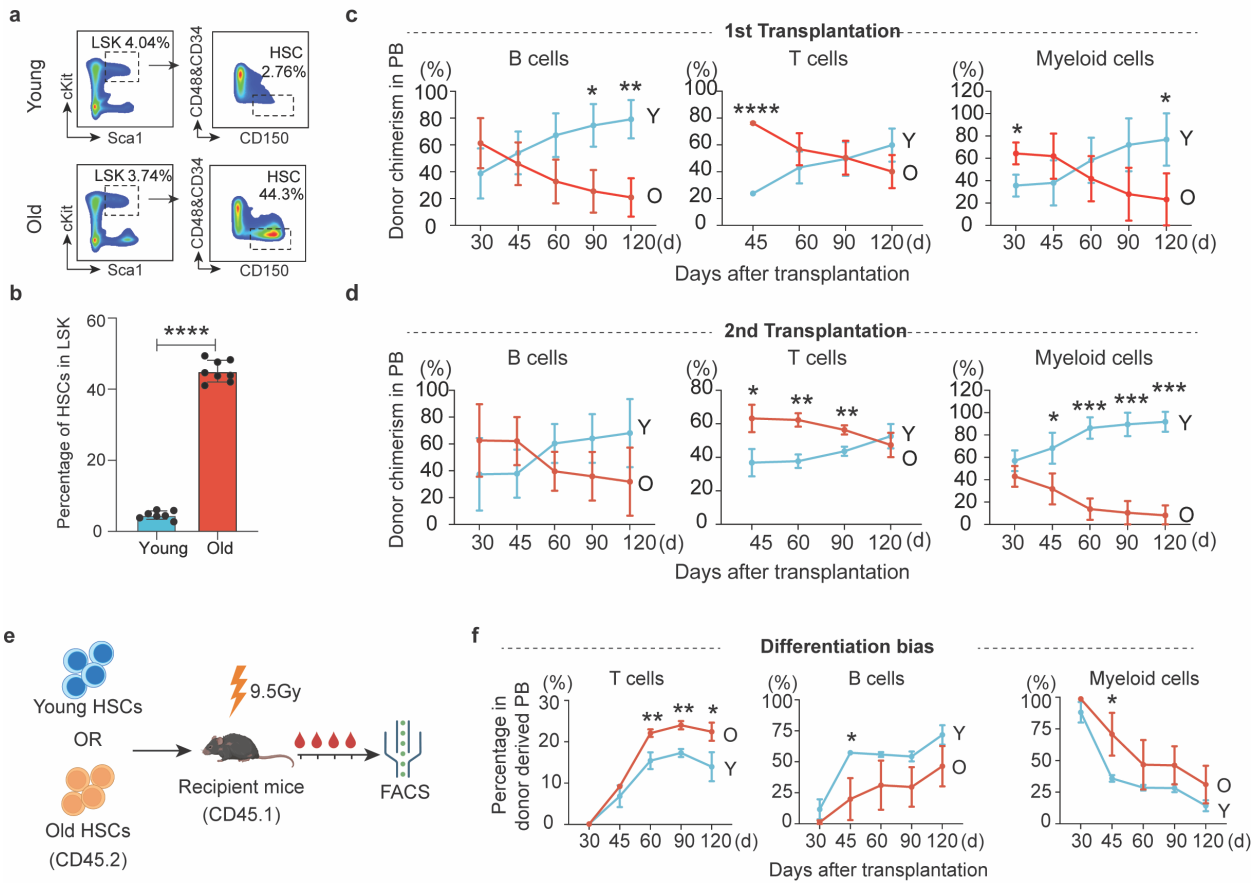

Extended Data Fig. 2

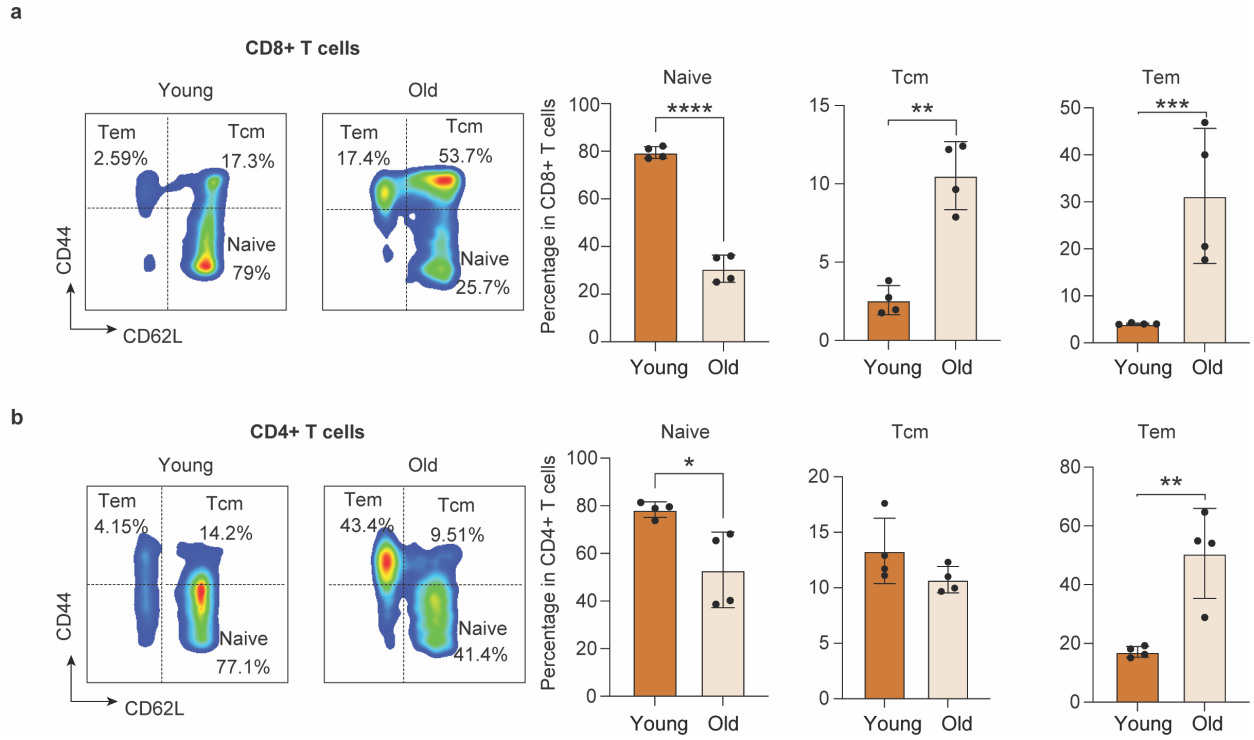

Extended Data Fig. 3

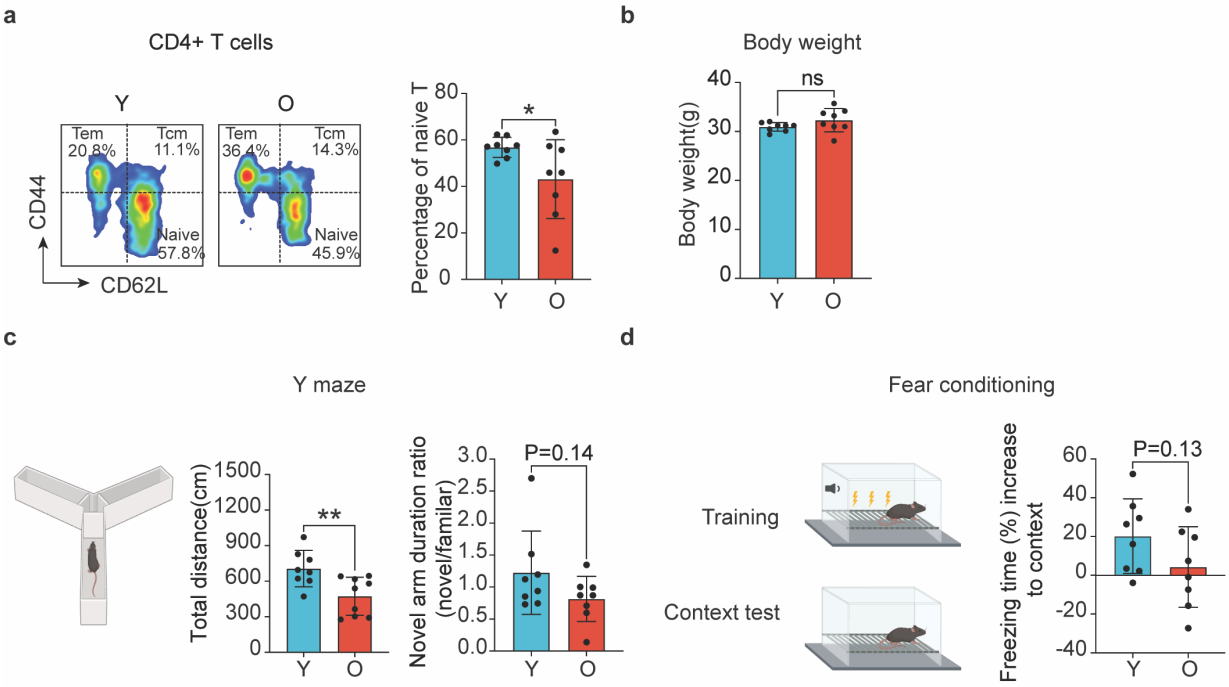

Extended Data Fig. 4

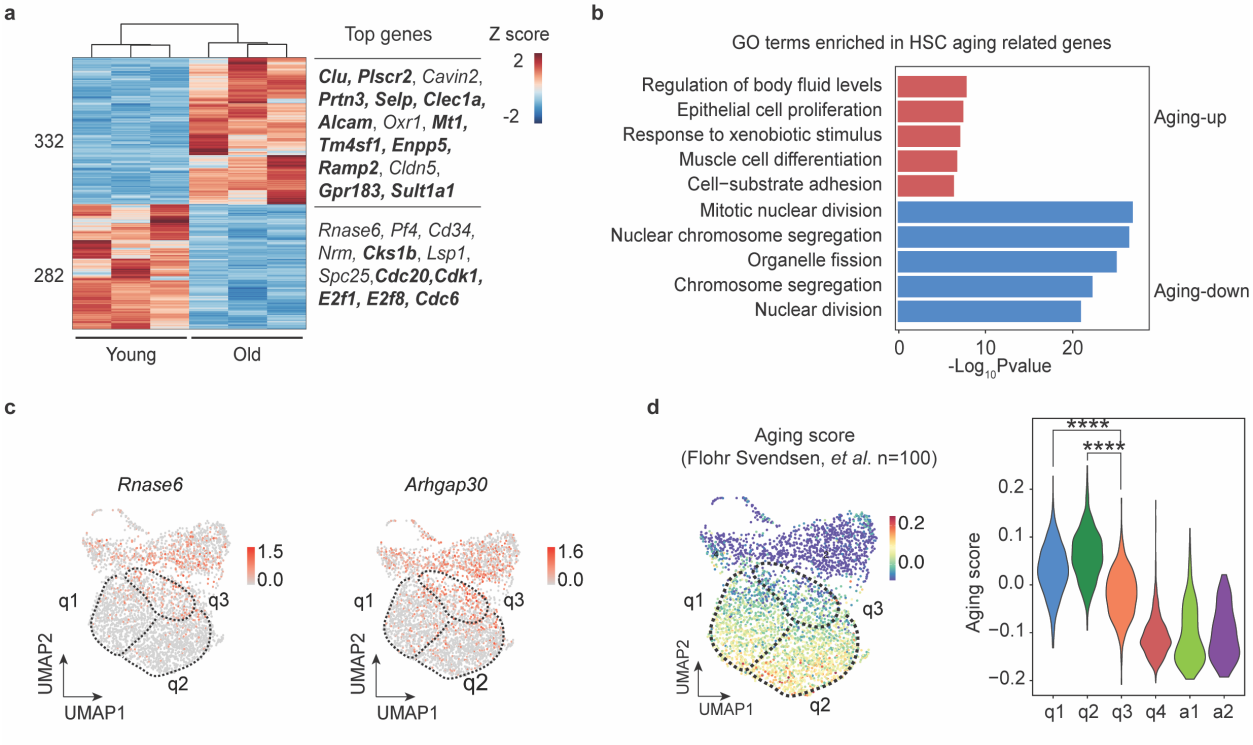

Extended Data Fig. 5

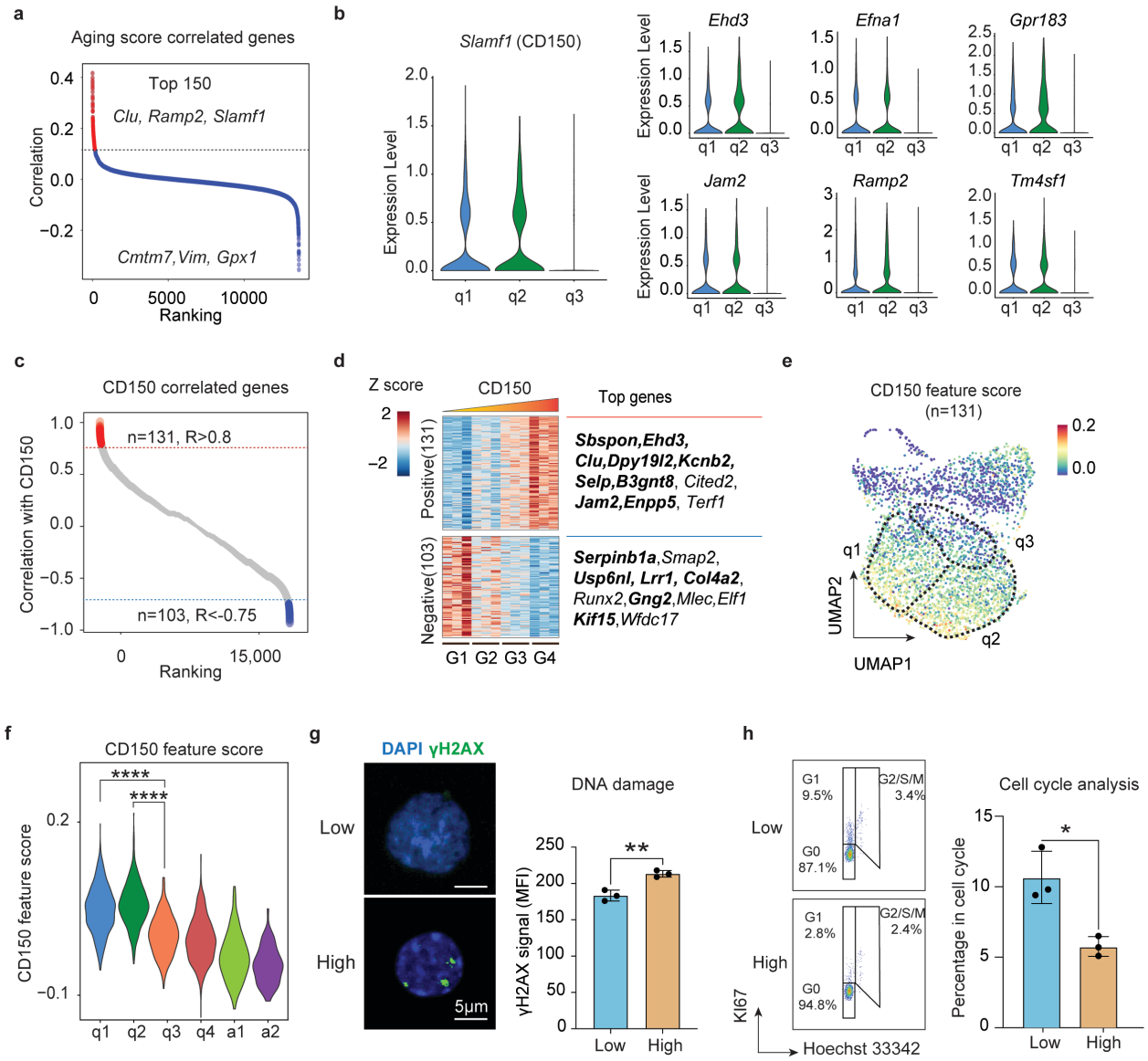

Extended Data Fig. 6

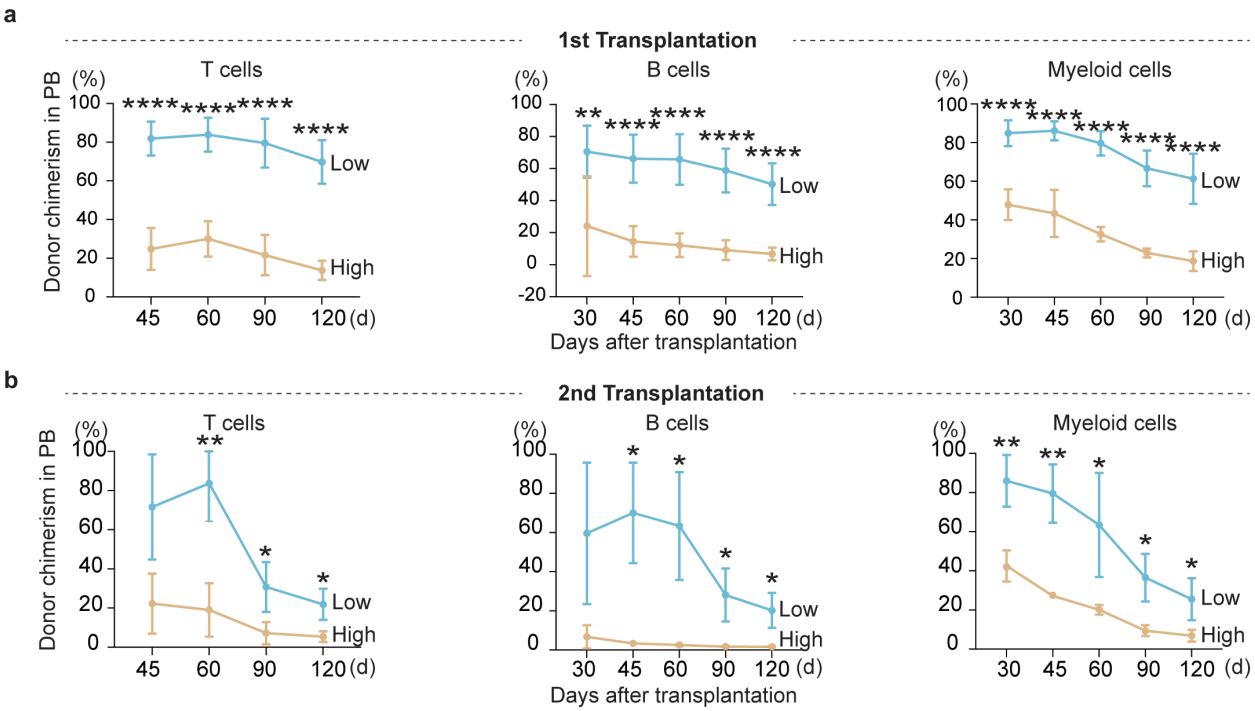

Extended Data Fig. 7

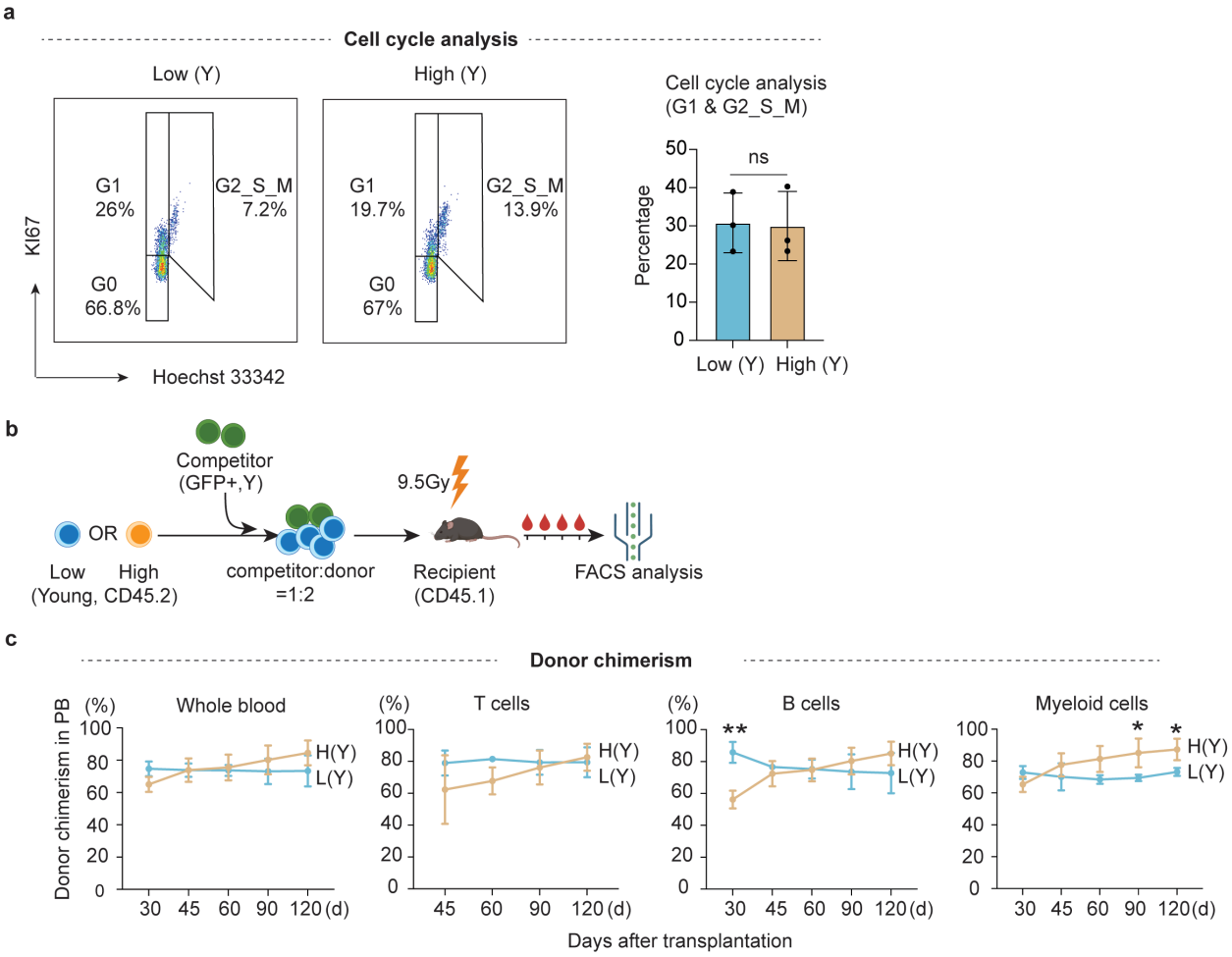

Extended Data Fig. 8

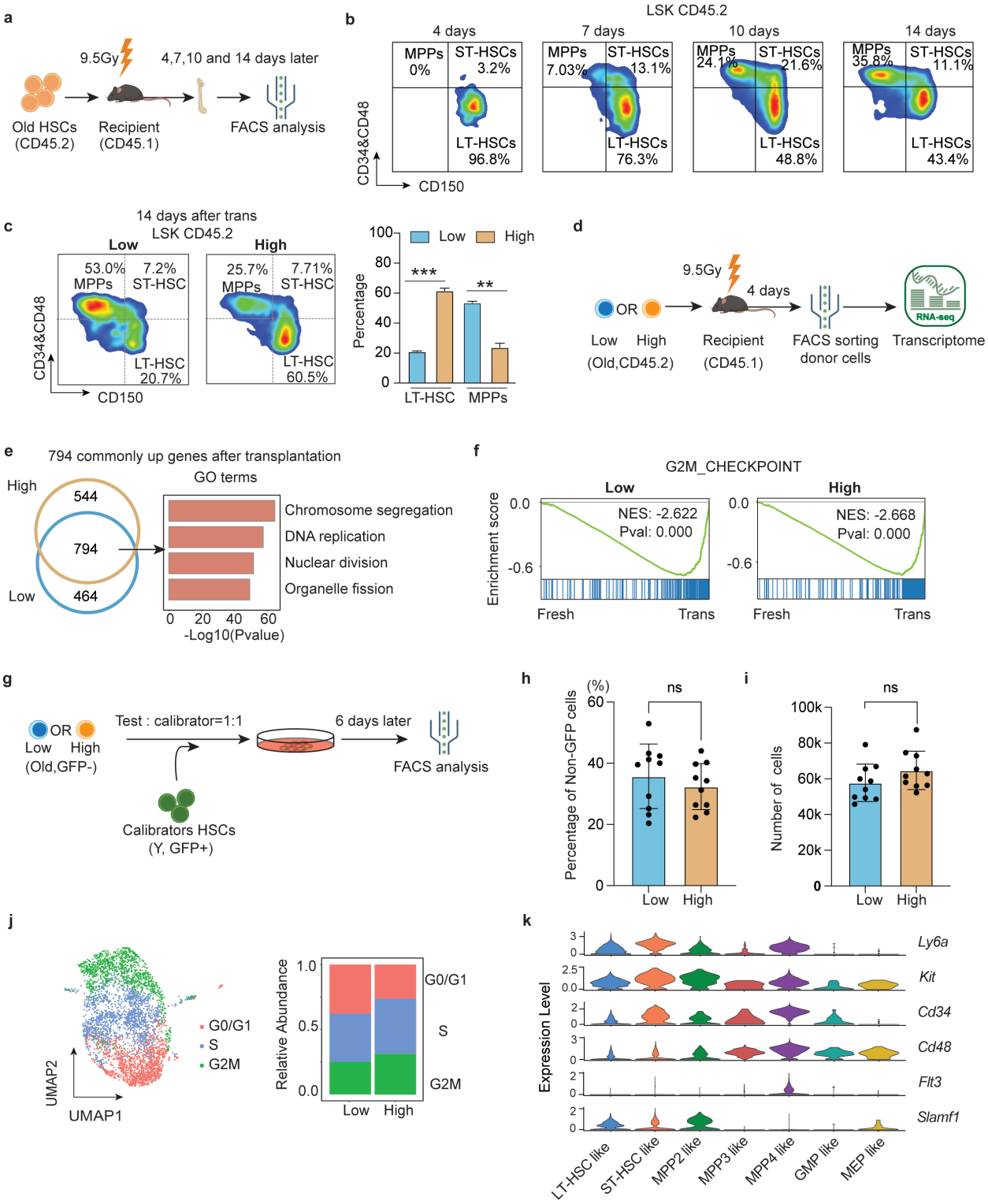

Extended Data Fig. 9

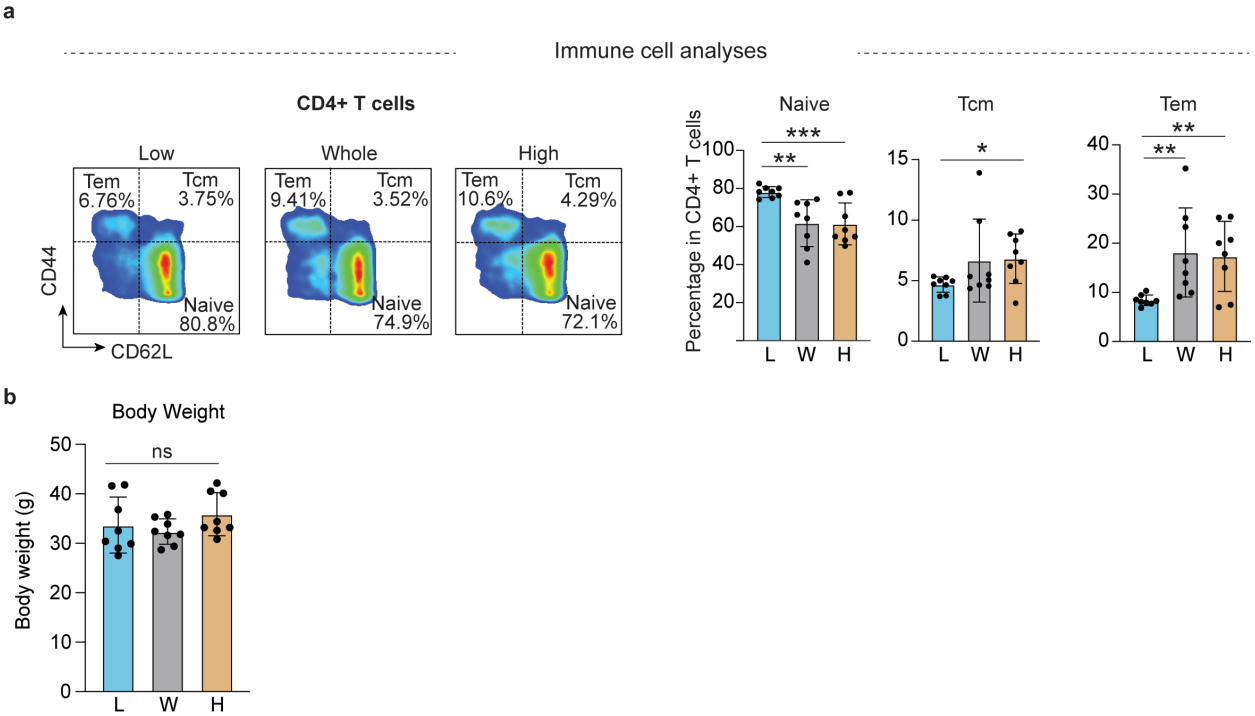
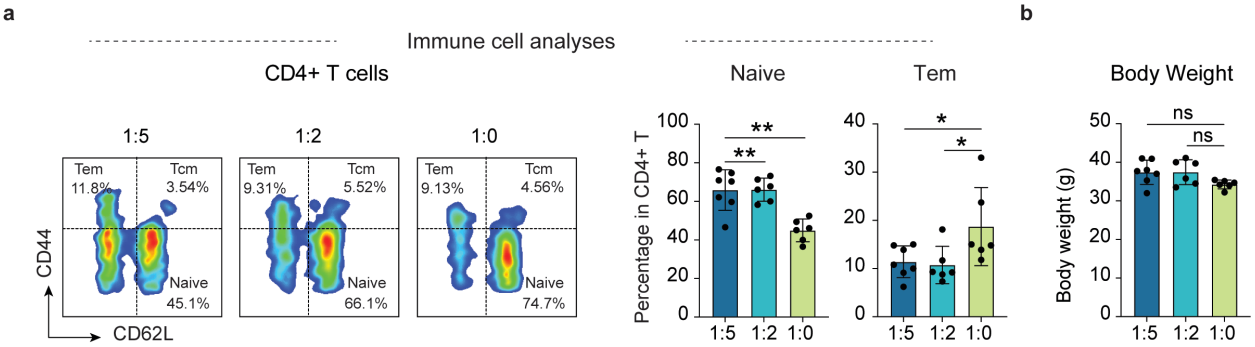
Extended Data Fig. 10